An evolutionary conserved lysine acetylation hotspot regulates plant mitochondrial malate dehydrogenase activity

Manuel Balparda[1*], Marlene Elsässer[2,3*], Mariana Badia[1,4*], Jonas Giese[5], Meike Hüdig[1], Lisa Reinmuth[2], Markus Schwarzländer[3], Iris Finkemeier[5#], Mareike Schallenberg-Rüdinger[2#], Veronica G. Maurino[1#]

[1]Molecular Plant Physiology, Institute of Molecular Physiology and Biotechnology of Plants (IMBIO), University of Bonn, Kirschallee 1, 53115 Bonn, Germany.

[2]Molecular Evolution, Institut für Zelluläre und Molekulare Botanik (IZMB), Rheinische Friedrich-Wilhelms-Universität Bonn, Kirschallee 1, 53115 Bonn, Germany

[3]Plant Energy Biology, Institute of Plant Biology and Biotechnology (IBBP), University of Münster, Schlossplatz 8, 48143 Münster, Germany

[4]Plant Molecular Physiology and Biotechnology Division, Institute of Developmental and Molecular Biology of Plants, Heinrich Heine University, and Cluster of Excellence on Plant Sciences (CEPLAS), Düsseldorf, Germany.

[5]Plant Physiology, Institute of Plant Biology and Biotechnology (IBBP), University of Münster, Schlossplatz 7, 48149 Münster, Germany

Running title: **Lysine acetylation of plant mitochondrial malate dehydrogenase**

* These authors contributed equally to the work

Correspondence to: Veronica G. Maurino (vero.maurino@uni-bonn.de), Mareike Schallenberg-Rüdinger (mrueding@uni-bonn.de) and Iris Finkemeier (iris.finkemeier@uni-muenster.de)

Present address: M.B., Instituto de Biología Molecular y Celular de Rosario (IBR-CONICET), Universidad Nacional de Rosario, 2000 Rosario, Argentina.

Abstract

Plants need to be able to rapidly and flexibly adjust their metabolism to changes their immediate environment. Since this necessity results from the sessile lifestyle of land plants, key mechanisms of orchestrating central metabolic acclimation are likely to have evolved early. Here we explore the role of lysine acetylation as a posttranslational modification to directly modulate metabolic function. First, we generate a lysine acetylome of the early divergent land plant *Physcomitrium (Physcomitrella) patens*. We identify 638 lysine acetylation sites, which were predominant in the mitochondria and plastids. A comparison with different angiosperms, including *Arabidopsis thaliana*, pinpoints lysine acetylation as conserved strategy in land plants. We focus on modified enzymes involved in mitochondrial central metabolism and select the mitochondrial malate dehydrogenase (mMDH), which acts as a hub of plant metabolic flexibility. In *P. patens* we detected a unique lysine acetylated site located next to one of the four acetylation sites detected in *A. thaliana* mMDH1. We assessed the kinetic behavior of recombinant *A. thaliana* and *P. patens* mMDHs with site-specifically incorporated acetyllysines. While the sites K325, K329 and K334 do not show any changes in the catalytic properties as assessed by oxaloacetate reduction activity, acetylation of *A. thaliana* mMDH1 at K170 markedly decreases its activity and acetylation of *P. patens* mMDH1 at K172 increases it. In both cases, acetylation induces modifications of the turnover number of the enzymes, without modifying the affinity for the substrates. Homology modelling of the mMDH1 proteins reveals a hotspot of lysine acetylation that is distant from the active site and homomerisation interfaces but conserved in land plants. The data reveal lysine acetylation as a strategy to tune the enzymatic properties of central metabolic enzymes with likely impact on metabolic capacity and flexibility to underpin plant acclimation.

Introduction

Flux through central metabolism is particularly dynamic in plants and can change dramatically with changing external conditions or intrinsic demands. For instance, the tricarboxylic acid (TCA) cycle that is localized in the mitochondria can operate in a cyclic or non-cyclic mode depending on cell type and the demands for reducing power, ATP, or carbon skeletons (Sweetlove et al., 2010). Although glycolysis-derived pyruvate decarboxylation is considered the major entry point for carbon into the TCA cycle in most organisms, it is malate rather than pyruvate that acts as the main substrate for the TCA cycle under most circumstances (Sweetlove et al., 2010). As a result, mitochondrial malate dehydrogenase

(mMDH; EC 1.1.1.37) is a hub of several different primary metabolic functions, respiratory activities, and metabolic flexibility (Fig. 1). mMDH interconverts malate and oxaloacetate (OAA) using NAD^+ as co-substrate. *In vivo*, the direction of the reaction depends on the demands of the cells and the redox state of the NAD pool in the matrix (Fig. 1). Apart from its classical role in supporting the TCA cycle flux to generate OAA from malate for respiration, mMDH provides OAA for the synthesis of aspartate, and – indirectly - of citrate as precursor for nitrogen assimilation (Fig. 1) (Hanning and Heldt, 1993; Sweetlove et al., 2010). In illuminated leaves in particular, mMDH can also support metabolic flux in the opposite direction to oxidize NADH to NAD^+ for the photorespiratory glycine decarboxylase (Journet et al., 1981), and as part of the mitochondrial malate valve that connects the redox states of the NAD pools of the mitochondrial matrix and the cytosol, through the exchange of malate and OAA (Fig. 1) (Scheibe, 2004; Scheibe et al., 2005; Sweetlove et al., 2010).

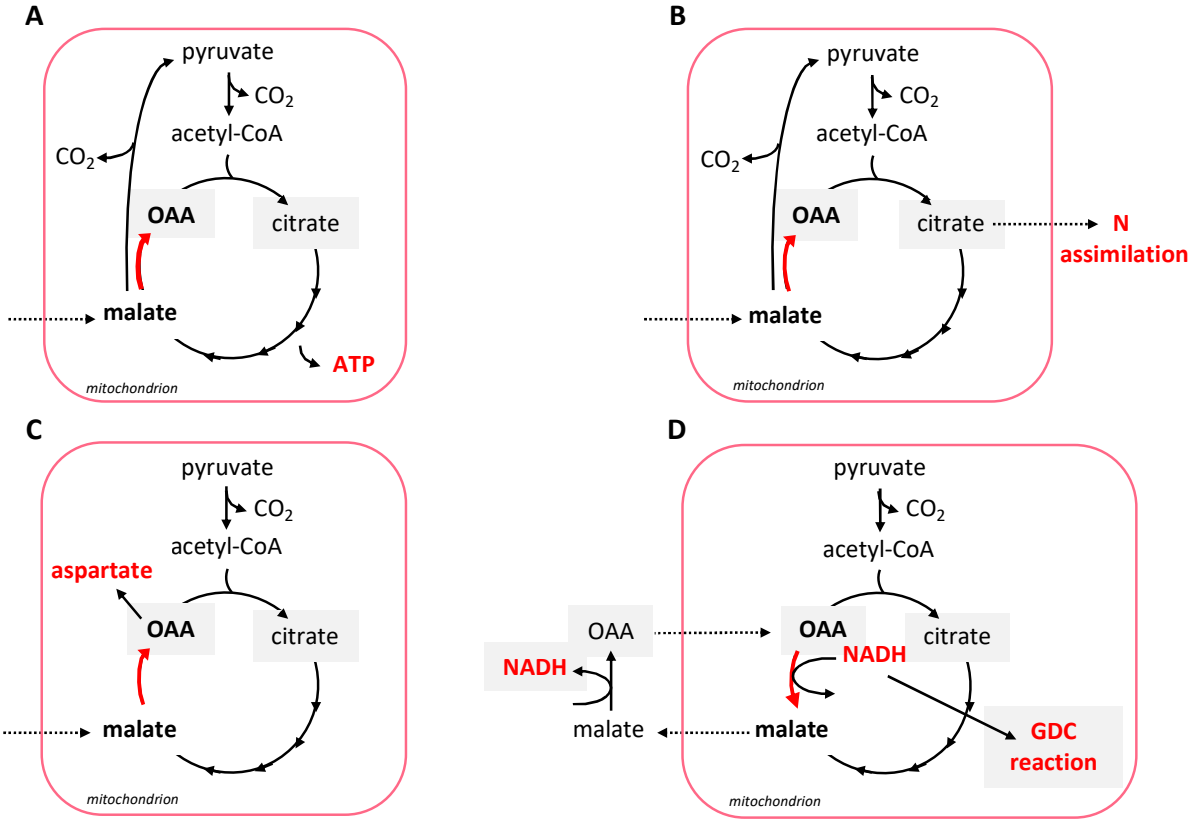

Figure 1. Direction of the mMDH reaction (red arrow) depending on the metabolic demands of the cells and the NAD redox state of the mitochondrial matrix. A. Catabolic mode of the TCA cycle. **B.** Provision of OAA for the synthesis of citrate as precursor for nitrogen assimilation. **C.** Provision of OAA for the synthesis of aspartate. **D.** Provision of NAD^+ for the photorespiratory glycine decarboxylase (GDC) and of malate for redox balance between matrix and cytosol. (Modified from Sweetlove et al., 2010).

Two isoforms, mMDH1 (AT1G53240) and mMDH2 (AT3G15020), are expressed in *A. thaliana,* of which mMDH1 is the main isoform in green tissue (Tomaz et al., 2010). While plant mMDH oligomerization state *in vivo* is not yet definitively established, pig heart mMDH is active as homodimer of ~70 kDa, possessing two equivalent binding sites (Murphey et al., 1967; Noyes et al., 1974; Shore and Chakrabarti, 1976; Gleason et al., 1994). Mitochondrial malate is not only metabolized through mMDH, but also via the NAD-dependent malic enzyme (NAD-ME) (Tronconi et al., 2008; Sweetlove et al., 2010; Maurino and Engqvist, 2015; Tronconi et al., 2020). Both enzymes together provide a remarkable degree of flexibility to plant respiratory metabolism, since they are able to supply mitochondrial carbon metabolism with substrate to respire, but also replenish the TCA cycle with carbon skeletons to maintain its function even when carbon skeletons are withdrawn for biosynthesis, e.g. of amino acids (Sweetlove et al., 2010). The central positioning of mMDH in the flexible primary carbon metabolism of plants makes a strict regulation of mMDH activity particularly likely. Nevertheless, relatively little is known about the regulation of mMDH enzymatic activities. Modulating of mMDH activity is not only critical to direct carbon flux either to OAA or pyruvate, but it also has the potential to set total (photo-) respiratory flux, by restricting carbon entry into the TCA cycle or NAD^+ provision to glycine decarboxylase, as well as to uncouple the redox states of the NAD pools of the matrix and the cytosol (Sweetlove et al., 2010). Plant mMDH was not found to be redox-regulated through the matrix thioredoxin system, but most probably controlled in response to variations in matrix adenine nucleotide balance, as its *in vitro* activity is lowered by ATP and inhibited by the increase in ATP/ADP ratio within the physiological range (Yoshida and Hisabori, 2016). Recently, in *A. thaliana* seedlings growing in liquid cultures and harvested at the beginning of the light period, mMDH1 was found to be acetylated at four different lysine residues: K170, K325, K329, and K334, respectively (König et al., 2014). Yet, the functional significance of those modifications has not been explored.

Posttranslational modifications (PTMs), such as phosphorylation and acetylation, can alter protein functions by affecting protein interactions, subcellular localization, or enzymatic activities (Matsuzaki et al., 2005; Yang and Seto, 2008; Ventura et al., 2010; Inuzuka et al., 2012; Bovdilova et al., 2019). Protein acetylation of lysine residues has long been recognized as regulator of transcriptional control (Allfrey et al., 1964). More recently, this PTM emerged as a regulator of cellular metabolism and signaling across different organisms (Wang et al., 2010; Zhao et al., 2010; Finkemeier et al., 2011; Choudhary et al., 2014; König et al., 2014).

Lysine acetylation has been found to be particularly widespread in bacterial and mitochondrial proteomes (Xu et al., 2009; Weinert et al., 2011). Two coenzymes of energy metabolism, acetyl-CoA and NAD^+, are required as substrates for the reversible acetylation of lysine residues (Imai et al., 2000; Lin et al., 2012). Acetyl-CoA is the coenzyme of lysine acetyltransferases but can also acetylate proteins non-enzymatically at a pH of higher than eight (Guan and Xiong, 2011; Hirschey et al., 2011; König et al., 2014). NAD^+ is used by sirtuin-type deacetylases, which also reside within mitochondria (Imai et al., 2000). In mitochondria, acetyl-CoA and NAD^+ play key roles as metabolic regulators. While, acetyl-CoA is produced in the mitochondrial matrix by the pyruvate dehydrogenase complex (PDC) and is oxidized in the TCA cycle, NAD^+ is required as electron acceptor in the TCA cycle. Respiration rates can have a major impact on protein acetylation, since changes in physiological NAD^+ concentration correlate with the activity of sirtuins (Lombard et al., 2007; Anderson et al., 2017). The mitochondrial acetylome of 10-day-old *Arabidopsis thaliana* seedlings revealed 120 lysine-acetylated proteins, which contained a total of 243 lysine-acetylated sites (König et al., 2014). Most TCA cycle enzymes of Arabidopsis were found to be acetylated, which parallels findings in animals and bacteria (Wang et al., 2010; Masri et al., 2013; König et al., 2014). The fact that PDC and most of TCA cycle enzymes were found lysine-acetylated across different organisms suggests that acetylation might represent an evolutionary conserved regulation system for TCA cycle function (Hosp et al., 2017).

Lysine acetylation is over-represented in both mitochondria and chloroplasts of angiosperm species, suggesting a prominent role of lysine acetylation in the direct modulation of the function of the endosymbiotic organelles (Hartl et al., 2017; Moller et al., 2020). Little is known about the conservation of acetylated lysines in distant land plant species, as investigations of lysine acetylation hitherto covered flowering plant species (Melo-Braga et al., 2012; König et al., 2014; Smith-Hammond et al., 2014; Fang et al., 2015; He et al., 2016; Zhen et al., 2016; Jiang et al., 2018) and a cyanobacterium (Mo et al., 2015), while comparative insights into other land plant clades is still lacking.

Here, we used the model moss *Physcomitrium (Physcomitrella) patens* as an early branching land plant to devise a comparative proteomic analysis to shed light on the evolutionary conservation of lysine acetylation in mitochondrial proteins and its potential functional diversification in plants. (Rensing et al., 2020). The analysis identified lysine acetylation of different mitochondrial proteins of *P. patens,* including mMDH. Using mMDH as a model

enzyme of central metabolic importance, we address the question of whether lysine acetylation represents an evolutionary conserved strategy to modulate mMDH activity. We synthesized acetylated mMDH at the specific lysine positions using the genetic code expansion strategy (Neumann et al., 2008) based on *A. thaliana* and *P. patens* mMDH isoforms, and assessed the kinetic behavior of the recombinant enzyme variants. Our observations pinpoint a hotspot of lysine acetylation that is likely to modulate mitochondrial carboxylic acid metabolism by fine tuning mMDH activity.

Results

Identification of mitochondrial lysine-acetylated proteins in *P. patens*

To identify lysine-acetylated proteins of *P. patens*, we analyzed the proteome of the gametophores of the moss via acetyllysine enrichment and liquid chromatography mass spectrometry (LC-MS/MS). Gametophores represent the haploid and dominant growth stage of mosses, which are analogous to the sporophyte growth stage of vascular plants (Strotbek et al., 2013). Overall, we detected 6428 proteins groups, of which 638 were found acetylated on at least one and at most nine lysines (Fig. 2, Supplementary Table 1).

We next classified the identified proteins according to their subcellular localization, making use of a previous analysis of the mitochondrial and plastid proteomes of *P. patens* (Müller et al., 2014). Additional proteins were grouped as organelle-localized when classified as such in the most recent annotation (Lang et al., 2018). In total, 1454 proteins were categorized as organellar proteins, and out of these, 331 proteins were acetylated (Fig. 2). Of those, 272 were annotated as plastid proteins and 98 as mitochondrial, including 39 proteins, which were classified as both plastidial and/or mitochondrial (Supplementary Table 2 and 3). A post-hoc manual inspection suggested that 16 out of the 98 putative mitochondrial proteins were rather plastidial (11) or peroxisomal (5; Supplementary Table 2) and the two putative plastidial citrate synthase protein isoforms were rather peroxisomal due to highest sequence similarity (65-74 %) to the peroxisomal citrate synthases 1, 2 and 3 of *A. thaliana*. Those considerations give rise to 52 mitochondrial, 30 mitochondrial or plastidial and 242 plastidial proteins being identified as lysine acetylated (Fig. 2). Similar to previous findings in angiosperms (Hartl et al., 2017; Moller et al., 2020), lysine acetylation is clearly overrepresented in the mitochondria and plastids of *P. patens* gametophores (Supplementary Table 2). In isolated mitochondria of Arabidopsis seedlings 120 acetylated proteins were identified (König et al., 2014). We observed an enrichment of lysine acetylated proteins in the TCA cycle enzyme

group, which also mirrors previous findings in *A. thaliana*. Lysine acetylation sites were detected on the TCA cycle enzymes aconitase, isocitrate dehydrogenase (both NAD- and NADP-dependent), 2-oxoglutarate dehydrogenase, and mMDH.

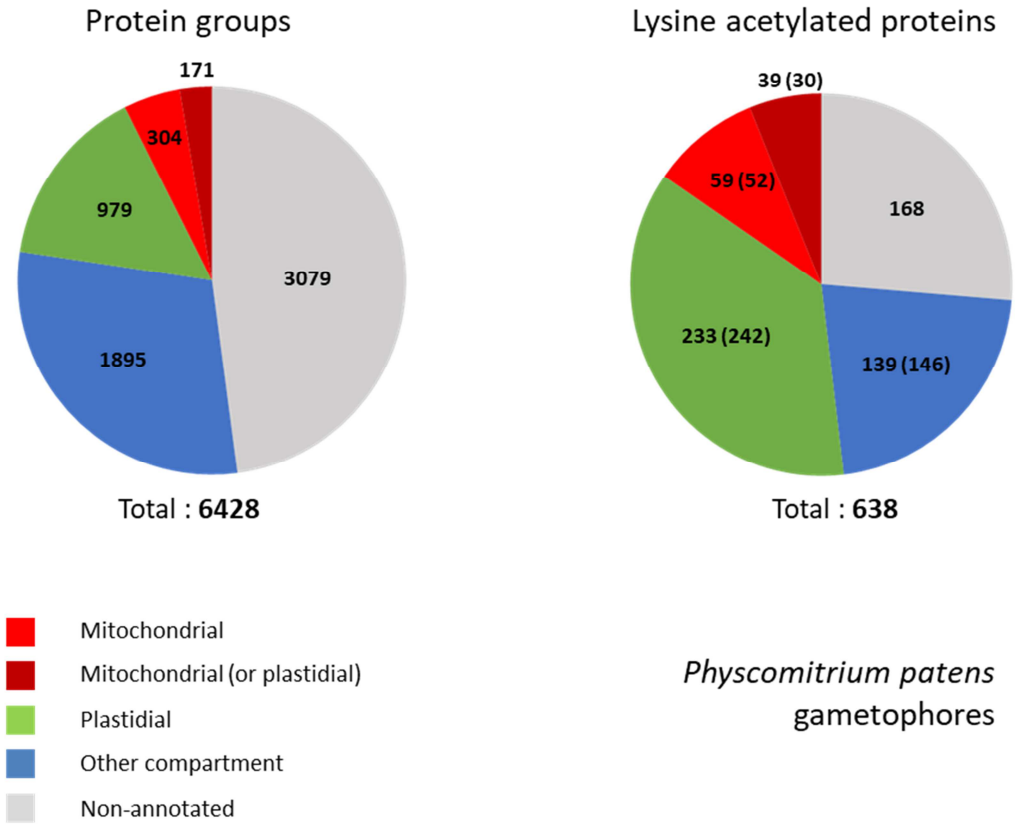

Figure 2: Distribution of lysine acetylation in *P. patens* proteins. Displayed are the proteins identified in gametophore samples of *P. patens* (left) and the proteins with detected acetylation sites (right). The proteins are classified as mitochondrial (red), plastidial (green), other compartment (blue) and non-annotated (grey) based on the localization identified in Müller et al. (2014) and the annotation provided by Lang et al. (2018). Proteins which could only be classified as mitochondrial or plastidial are displayed in dark red. Manually inspection suggested different localisation for 18 proteins; modified numbers are given in brackets. Organellar proteins are overrepresented in the lysine acetylation dataset.

Different lysine residues are acetylated in TCA cycle enzymes of *A. thaliana* and *P. patens*

The specific sites of lysine acetylation in TCA cycle enzymes and other mitochondrial proteins were compared between orthologous proteins of *P. patens* and *A. thaliana* (König et al., 2014). The PDC E1 α as well as four of the five identified TCA cycle enzymes were found to be acetylated in both *P. patens* and *A. thaliana* (Table 1). For NADP isocitrate dehydrogenase lysine acetylation was detected in *P. patens* only.

Table 1. Conservation of lysine acetylation between mitochondrial TCA cycle and PDC proteins identified in *A. thaliana* and *P. patens*. Proteins identified to be acetylated in *P. patens* and *A. thaliana* are organized into orthologous groups. Total numbers of identified acetylated lysines (K, total), number of acetylated Ks at different positions in the orthologous proteins (diff.), numbers of acetylated Ks with conserved lysines at same position of at least one putative ortholog of the other species (shared K) and shared acetylated lysines (shared acK) are listed separately. Positions of the acetylated Ks (acK) in the proteins are given and numbers are underlined, when Ks are conserved in the putative orthologs at this position. Bold numbers represent acetyated lysines, which were detected in at least one *P. patens* and one *A. thaliana* putative ortholog of both datasets. The malate dehydrogenase proteins shown in red are further assessed in this study. Pp: *P. patens*, AT: *A. thaliana.*

		Number of acetylated lysines				
Orthologous protein group	**Accession No.**	**total**	**diff.**	**shared K**	**shared acK**	**Position(s) of acK(s)**
Pyruvate dehydrogenase complex E1 α	AT1G24180.1	2	2	1	1	**85**;336
	AT1G59900.1	2				**81**;332
	Pp3c12_7580V3.1	1				**86**
	Pp3c4_20210V3.1	1				**86**
Aconitase (TCA)	AT2G05710.1	3	7	5	1	**790**;846;895
	AT4G26970.1	2				**795**;900
	Pp3c15_25170V3.1	5				520;529;598;**803**;844
	Pp3c9_25990V3.2	2				491;806
2-oxoglutarate dehydrogenase E1 (TCA)	AT3G55410.1	3	5	2	0	549;599;613
	AT5G65750.1	2				603;873
	Pp3c23_7750V3.1	1				1000
NAD isocitrate dehydrogenase (TCA)	AT3G09810.1	1	3	3	0	181
	AT5G03290.1	2				181;218
	Pp3c15_3920V3.1	1				365
	Pp3c9_4370V3.1	1				355
Malate dehydrogenase (TCA)	**AT1G53240.1/mMDH1**	4	5	3	0	170;325;329;334
	AT3G15020.1/mMDH2	1				170
	Pp3c4_20940V3.1/MDH1	1				172
	Pp3c12_8120V3.1/mMDH2	1				170
Sum	**AT: 10/Pp: 9**	**36**	**22**	**14**	**2**	

Altogether 22 different lysine residues were found to be acetylated in the four TCA cycle enzymes and the E1 α subunit of the PDC in *P. patens* or *A. thaliana*. In 14 of the 23 positions, the lysine, acetylated in one species, was conserved in at least one orthologous protein of the other species. Only the E1 α subunit of the PDC and the Aconitase of both species shared a lysine that was acetylated in both datasets (Table 1). A similar picture emerged for the other orthologous protein groups investigated (Supplementary Table 4). Orthologous proteins of *A. thaliana* and *P. patens* showed conserved lysine positions, but for each individual, such lysine acetylation was typically detected in one of the two species only (Table 1, Supplementary Table 4).

We found 35 *A. thaliana* proteins and 40 *P. patens* proteins classified into 22 orthologous groups. Each group consists of one up to six different proteins per species, depending on the number of paralogous proteins encoded in the genome and found in the datasets. 121 lysines at different positions were found to be acetylated in at least one protein of the orthologous

groups. While 80 of these 121 positions carried a lysine in the orthologous proteins of the respective other species as well, 14 acetylated lysines were detected at same positions in orthologous proteins of both species (Supplementary Table 4).

A. thaliana mMDH1 was found acetylated on four lysines (K170, K325, K329, and K334) (König et al., 2014), while *P. patens* mMDHs were acetylated in one unique lysine (K172 of Pp3c4_20940V3.1, in the following named mMDH1, or K170 of Pp3c12_8120V3.1, in the following named mMDH2) corresponding to K169 of *A. thaliana* mMDH1 (Table 1, Fig. 3). Acetylation sites K170 of *A. thaliana* mMDH proteins and K172 of *P. patens* mMDH proteins could not be unequivocally assigned to one of the two paralogs, mMDH1 and mMDH2, present in each species. However, in the proteomic datasets mMDH1 of *A. thaliana* and mMDH1of *P. patens* were more abundant than the respective second paralogs, *A. thaliana* mMDH2 and *P. patens* mMDH2 (Supplementary Table 1, König et al. 2014). We hence focused our further analyses on the dominant mMDH1 protein of both species.

Lysine acetylation of mMDH along land plant phylogeny

To analyse if acetylation of mMDH is common in land plants, we further inspected available acetylome datasets of ten additional plant species, all of which flowering plants, for the presence of acetylation sites in mMDH (Supplementary Table 5). In six of the ten species, unique acetylated peptides of mMDHs were detected (Fig. 3, Supplementary Fig. 1, Supplementary Table 5). The species, for which information on MDH acetylation is available, cover six different orders of flowering plants (*A. thaliana*: Brassicales (König et al. 2014), *Fragaria ananassa*: Rosales (Fang et al., 2015), *Pisum sativum:* Fabales (Smith-Hammond et al. 2014), *Vitis vinifera:* Vitales (Melo-Braga et al., 2012), *Camellia sinensis:* Ericales (Jiang et al. 2018), *Oryza sativa* and *Brachypodium distachyon:* Poales (He et al., 2016; Zhen et al., 2016; Jiang et al., 2018).

To get a better picture of the conservation of the lysines and known acetylation sites of mMDH along the land plant phylogeny, we aligned the mMDH protein sequences of the six species with mMDHs of model plants representing each main land plant clade, including *P. patens* and *A. thaliana* (Fig. 3). We obtained the protein data via Blast using the *A. thaliana* mMDH1 as query against different databases. MDH proteins, which clustered together with the mitochondrial MDH proteins of *A. thaliana* and *P. patens* in a Neighbor joining and Maximum likelihood phylogeny performed in parallel, were identified for all major land

plant species (Supplementary Fig. 1). Peroxisomal and chloroplastic MDHs of *A thaliana* and *P. patens* clustered in separate clades. For comparison the *E. coli* MDH and human mMDH2 with lysine acetylation in diverse positions (Fig. 3) (Wang et al., 2010; Schilling et al., 2015) were included in the alignment. Sequences were ordered based on the common land plant phylogeny (Qiu et al., 2006; Group, 2009). Only for *Oryza sativa* different acetylation sites in two mMDHs paralogs were identified and both proteins were included in the alignment (He et al., 2016) (Fig. 3).

We displayed the acetylation sites found in mMDH isoforms of each species in the alignment. As a result, we identified two neighboring lysine residues in the mMDH sequences that correspond to K169 and K170 in the *A. thaliana* sequence (Fig. 3). Interestingly, these lysine residues were found acetylated in mMDHs of several plant species (Fig. 3). K172 of *P. patens* mMDH1 (corresponding to K169 of *A. thaliana*), identified with high coverage in the *P. patens* acetylome, was also lysine acetylated in *Camellia* leaves and *Brachypodium* seedling leaves (Zhen et al., 2016; Jiang et al., 2018). K170 of *A. thaliana* mMDH was also acetylated in strawberry leaves (Fang et al., 2015) and in grape vine mesocarp and exocarp after induction with *Lobesia botrana* (Melo-Braga et al., 2012) (Fig. 3). Interestingly, in rice mMDH2 the lysines at position 169 and 170 were found to be differentially acetylated in diverse organs. K169 was found acetylated in leaves (Lu et al., 2018), whereas K170 was detected as acetylated in embryos (He et al., 2016). All other angiosperms in this dataset showed acetylation only on one or the other K (Fig. 3).

Interestingly, all other investigated species either show a lysine or an arginine, which is similar in structure to the non-acetylated lysine, at these two positions. Even in the plastid and peroxisomal MDHs of *Arabidopsis thaliana* and *P. patens*, either a lysine or an arginine is present at these two positions (Supplementary Table 4). The peroxisomal pMDH1 of *A. thaliana* shares the acetylation site with the *P. patens* mMDH1 (Supplementary Fig. 1, Supplementary Table 4, (König et al., 2014). In the *E. coli* MDH and human MDH, however, position 169 shows an asparagine, which would partially mimic the constantly acetylated lysine. Other acetylated lysines in *A. thaliana* MDH1 are K325, K329, and K334 (König et al., 2014). While K325 was exclusively found to be acetylated in *A. thaliana* thus far, K329 was also found acetylated in *Oryza sativa* and in *E. coli*.

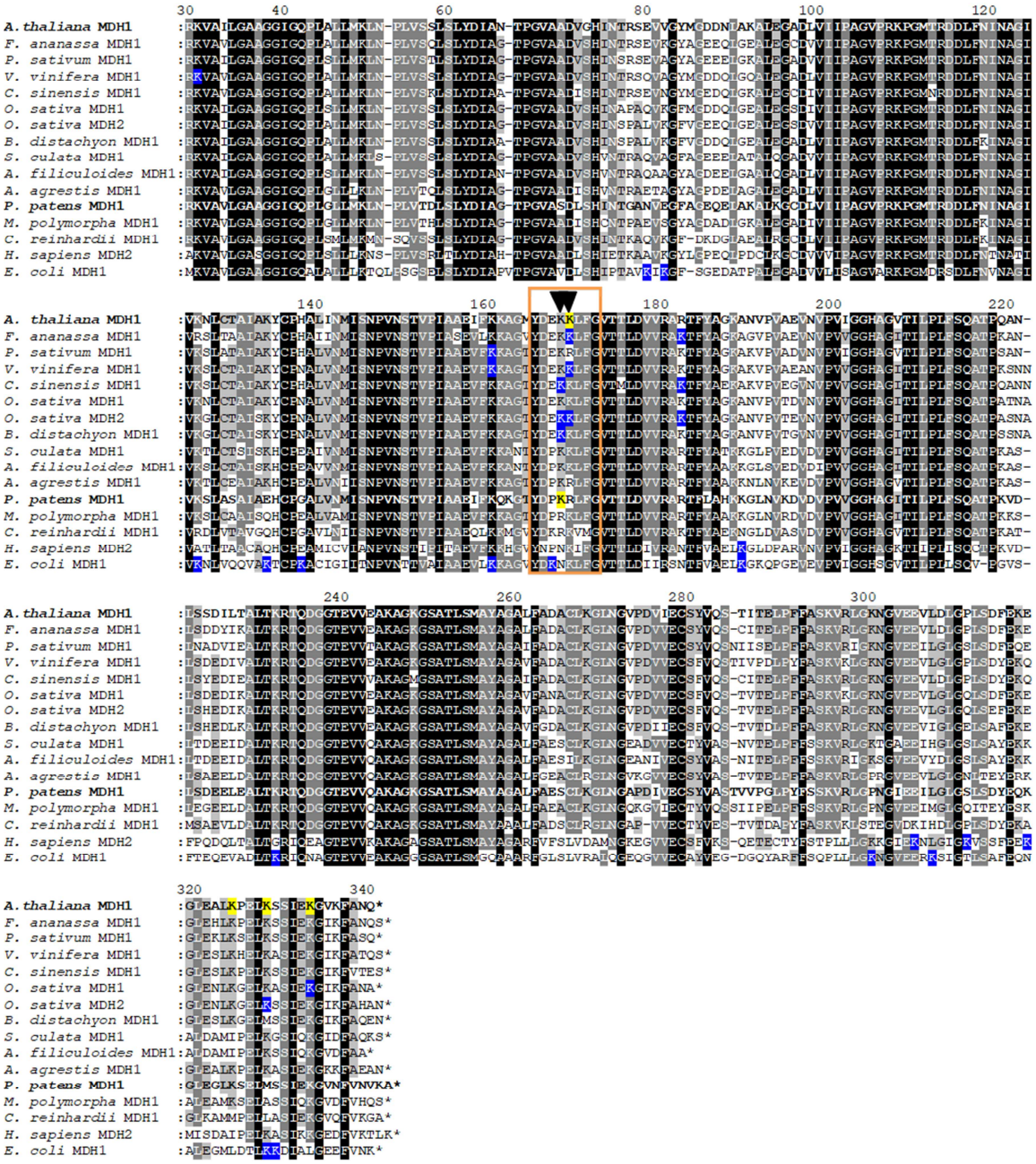

Figure 3. Sequence conservation of mMDH of selected land plant species, human and *E. coli* and their lysine acetylation sites. Alignment of the acetylated protein isoforms of the mMDHs of the angiosperms *A. thaliana*, *C. sinensis*, *V. vinifera*, *P. sativum*, *F. ananassa*, *B. distachyon* and *O. sativa* with known lysine acetylation sites marked in blue. Orthologues of representative species of other major land plant clades (the green algae *C. reinhardtii*, the liverwort *M. polymorpha*, the moss *P. patens*, the hornwort *A. agrestis* and the ferns *A. filiculoides* and *S. cucullata*) share high sequence conservation. Shading in black indicates 100 %, in dark grey 80 % and in light grey 60% amino acid identity conservation. Sequences are ordered based on the common land plant phylogeny (Qiu et al., 2006; Group, 2009). The sequences of *H. sapiens* mitochondrial MDH2 and *E. coli* MDH with their identified acetylated lysines (blue) are included for comparison. The numbering is based on the sequence of MDH1 of *A. thaliana*. The alignment starts from amino acid 30 which corresponds to the start methionine of *E. coli* MDH. Yellow highlighted Ks are acetylated lysines in *A. thaliana* and *P. patens* mMDH1 analyzed in this study. A region with acetylation sites conserved in different species is framed in orange and includes position K169 and K170 marked with black arrows.

Production of site-specific acetylated *A. thaliana* and *P. patens* mMDH1 proteoforms and analysis of their enzymatic properties

The conservation of lysine acetylation sites found in plant mMDH (Fig. 3) prompted us to investigate the influence of acetylation on the enzymatic properties of the enzyme in the model plants *A. thaliana* and *P. patens*. We selected the lysines K170, K325, K329, and K334 of mMDH1 of *A. thaliana* (König et al., 2014) as well as the K172 of mMDH1 of *P. patens* (Table 1, Fig. 3, Supplementary Tables 2 and 3) to selectively incorporate acetyl lysine (AcK) at these positions and to analyze the effect of the modification on the kinetic properties of the enzymes *in vitro*. The lysine acetylation was incorporated into recombinantly expressed proteins using the amber suppression system in *E. coli*, which allows the co-translational addition of N-acetyl lysine in response to a stop codon at the desired positions (Neumann et al., 2008; Neumann et al., 2009). Wild-type *A. thaliana* and *P. patens* mMDH1 and the protein versions carrying the single acetylated lysines were expressed in *E. coli*, in the presence of N-acetyl lysine and nicotinamide (to inhibit the *E. coli* deacetylase CobB) and purified to homogeneity (Fig. 4A). In all cases we obtained proteins of the expected molecular masses (33.5 kDa in the case of *A. thaliana* and 36 kDa for *P. patens*; Fig. 4A). The incorporation of AcK at the desired positions of *A. thaliana* and *P. patens* mMDH1 was confirmed by LC-MS/MS.

The purified recombinant wild-type mMDH1 and the single acetylated versions were used to determine the kinetic parameters. We focused on the mMDH activity in the direction of the reduction of OAA as the acetylated lysines were identified in *A. thaliana* seedlings during the light period, where mMDH activity predominantly is needed to produce malate for its translocation to the cytosol for redox balance (Fig. 1D). We found that acetylation at positions K325, K329, and K334 in *A. thaliana* mMDH1 had no significant effects on the turnover number (k_{cat}) and the affinity to OAA (K_{mOAA}) compared to wild-type. In contrast, the acetylation at K170 decreased the turnover number to 37% compared to the wild-type. The same analysis with *P. patens* mMDH1 indicated that the acetylation in K172 provokes an increase in the turnover number of 101% in comparison to the wild-type (Fig. 4B).

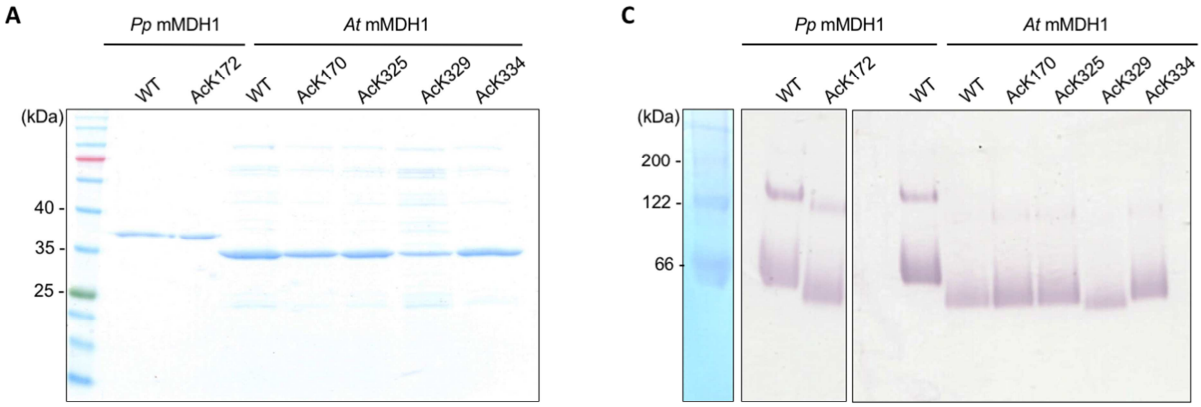

B

	A. thaliana					*P. patens*	
	WT	AcK170	AcK325	AcK329	AcK334	WT	AcK172
K_{mOAA} (µM)	17 ± 7	9 ± 3	20 ± 12	17 ± 4	18 ± 6	18 ± 8	23 ± 10
k_{cat} (s^{-1})	548 ± 111[a]	**204 ± 32.8[b]**	471 ± 208[a]	484 ± 130[a]	353 ± 18[a]	265 ± 17[a]	**533 ± 40[b]**

Figure 4. The impact of lysine acetylation on mMDH activity. **A.** SDS-PAGE stained with Coomassie of the isolated recombinant wild-type (WT) and lysine acetylated (AcK) variants of *P. patens* (*Pp*) and *A. thaliana* (*At*) mMDH1. To the left, molecular weight markers (Spectra Multicolor Broad Range Protein Ladder; ThermoFisher Scientific). **B.** Kinetics parameters of the oxidation of OAA by recombinant wild-type (WT) and lysine-acetylated (AcK) versions of *A. thaliana* and *P. patens* mMDH1. Data were adjusted to Michaelis-Menten equation by non-lineal regression with Prism 6 (GraphPad Software). The values represent the mean ± standard deviation; n=at least three independent enzyme preparations, each measured at least in triplicate. Values in bold are statistically significantly different from the corresponding wild-type (WT) evaluated by one-way ANOVA and Dunnett's test in the case of *A. thaliana* (k_{cat} p=0.0406) and unpaired t-test in the case of *P. patens* (K_{cat} p=0.0004). a=statistically similar values, b=significant difference to the other values. **C.** Native PAGE of recombinant wild-type (WT) and lysine-acetylated (AcK) variants of *P. patens* (*Pp*) and *A. thaliana* (*At*) mMDH1.

Mobility analysis of the acetylated proteins by native PAGE

The introduction of a PTM can cause changes in structural features of a protein, which can impact the kinetic properties. To analyse if the organization of the wild-type enzymes is maintained in the single acetylated mMDH recombinant variants produced, we compared the mobility of the enzymes in native gel electrophoresis. The isolated proteins were run side-by-side on the same gel and the gel was analyzed for MDH activity.

We found that in native PAGE the recombinant wild-type mMDH1 of *A. thaliana* and *P. patens* are active in two oligomeric arrangements that most likely correspond to dimers and tetramers (Fig. 4C). Under the conditions of our *in vitro* assay the dimeric form was more abundant than the tetrameric form, which corresponds to observations made by BN-PAGE of

mitochondrial extracts from *A. thaliana* leaves (Senkler et al., 2017). The wild-type mMDH1 proteins of *A. thaliana* and *P. patens* differ slightly in the mobility of both oligomeric states, which is likely due to the differences in the molecular masses of the subunits (Fig. 4A) and of different gross shapes of the proteins that can be adopted in solution.

We found that in native PAGE all acetylated mMDH1 versions of *A. thaliana* and *P. patens* conserved the same oligomeric arrangements observed in the wild-type proteins (Fig. 4C), indicating that the detected activity changes cannot be accounted for by changes in homomerisation. The mobilities of the proteins in both oligomeric states were similar in the case of *A. thaliana* wild-type and the acetylated proteins, including AcK170, which presented a significant decrease in turnover number (Fig. 4B). Interestingly, the *P. patens* AcK172 version showed a slightly enhanced mobility with regards to the corresponding wild-type (Fig. 4C), indicating that the incorporation of the acetyl group at K172 slightly modifies the mobility of both oligomeric states of the protein in native PAGE.

Mapping of acetylation sites on the crystal structures of MDH

We used the crystal structures of *E. coli* MDH (PDB ID:1EMD) and human MDH2 (PDB ID: 2DFD) to perform homology modelling of the *A. thaliana* and *P. patens* structures and to map the acetylated lysine residues found in this study. Models of the *A. thaliana* and *P. patens* mMDH1 monomers, dimers and tetramers show that the acetylated lysine residues are neither located in the direct vicinity of the active site (Fig. 5A-B) nor of the dimer or tetramer interfaces predicted by the constructed models (Fig. 5C-F).

Superposition analysis of the monomeric structures suggest that *A. thaliana* K170, *P. patens* K172 and *E. coli* 140 are located in the same region of the three-dimensional structure of the proteins (Fig. 6A-C), indicating conservation of the regulatory function of these lysine residues. The specific spatial orientation of the lysine side chains may differ from the orientations observed in the structures of *A. thaliana* and *P. patens*, however, since the shown structures are modelled based on the crystal structures of *E. coli* and human MDH.

In addition, K329 of *A. thaliana* mMDH1 show spatial identity with K300 of *E. coli* MDH (Fig. 6B, D). The superposition of the structures indicates that all acetylated lysine residues of *A. thaliana* and *P. patens* mMDH1 are located in different regions of the protein surface than those of human mMDH2 (Fig. 6E), pinpointing differences in the regulation strategy in plants and humans.

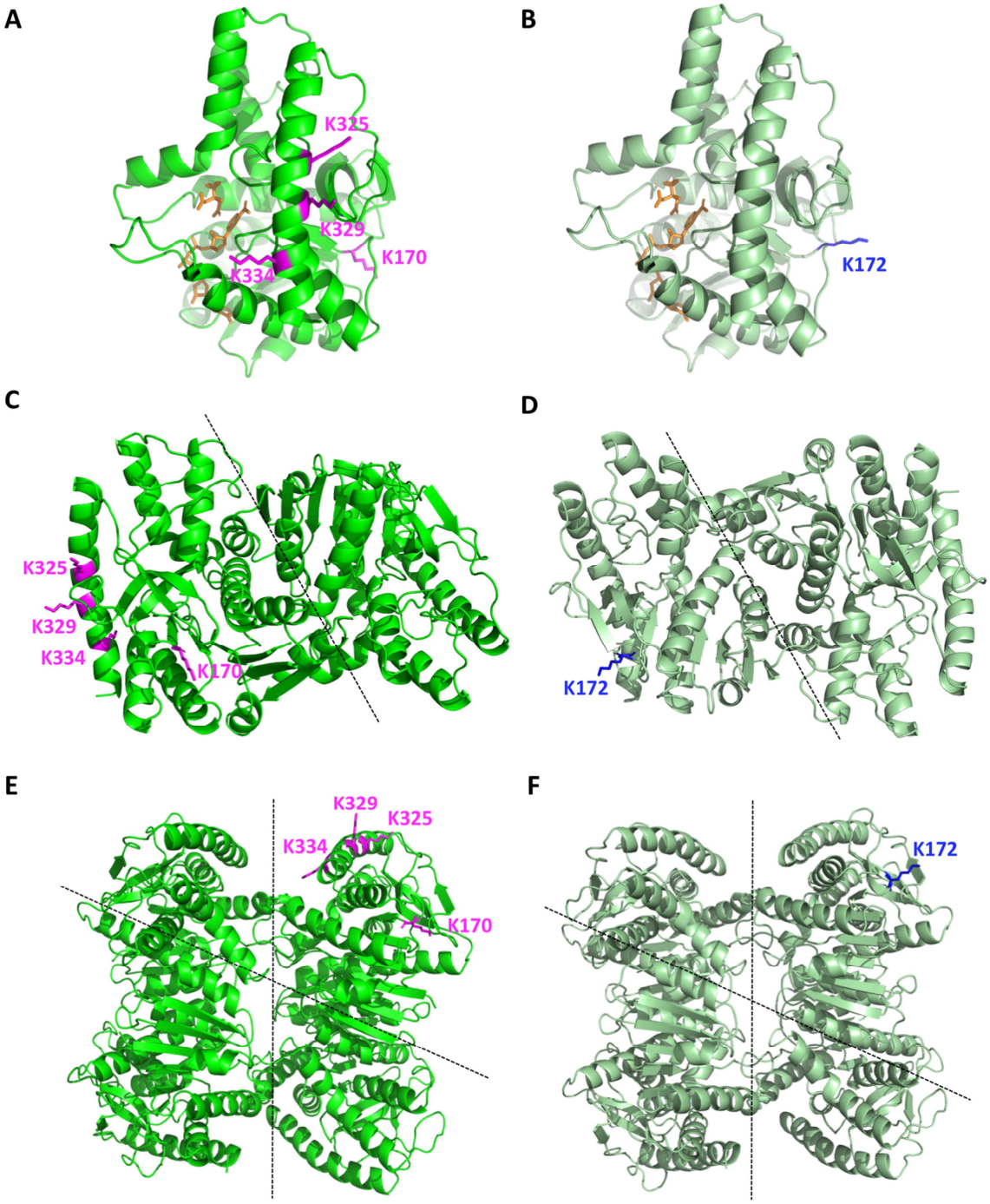

Figure 5. Structures of *A. thaliana* and *P. patens* mMDH1 as obtained by homology modelling. Structures of *A. thaliana* (bright green **A, C, E**) and *P. patens* (dark green; **B, D, F**) mMDH1 modelled as monomers (A and B), dimers (B and D), and tetramers (E and F). The structures were modelled using the crystal structure of *E. coli* MDH (PDB ID:1EMD) and human MDH2 (PDB ID: 2DFD). The acetylated lysine residues of *A. thaliana* mMDH1 are shown in magenta. The acetylated lysine residue of *P. patens* mMDH1 is shown in blue. In A and B, the ligand molecules NAD^+ and citrate - in brown - were manually fitted in by aligning the structure of the *H. sapiens* MDH2. Dotted lines indicate the dimer and tetramer interfaces.

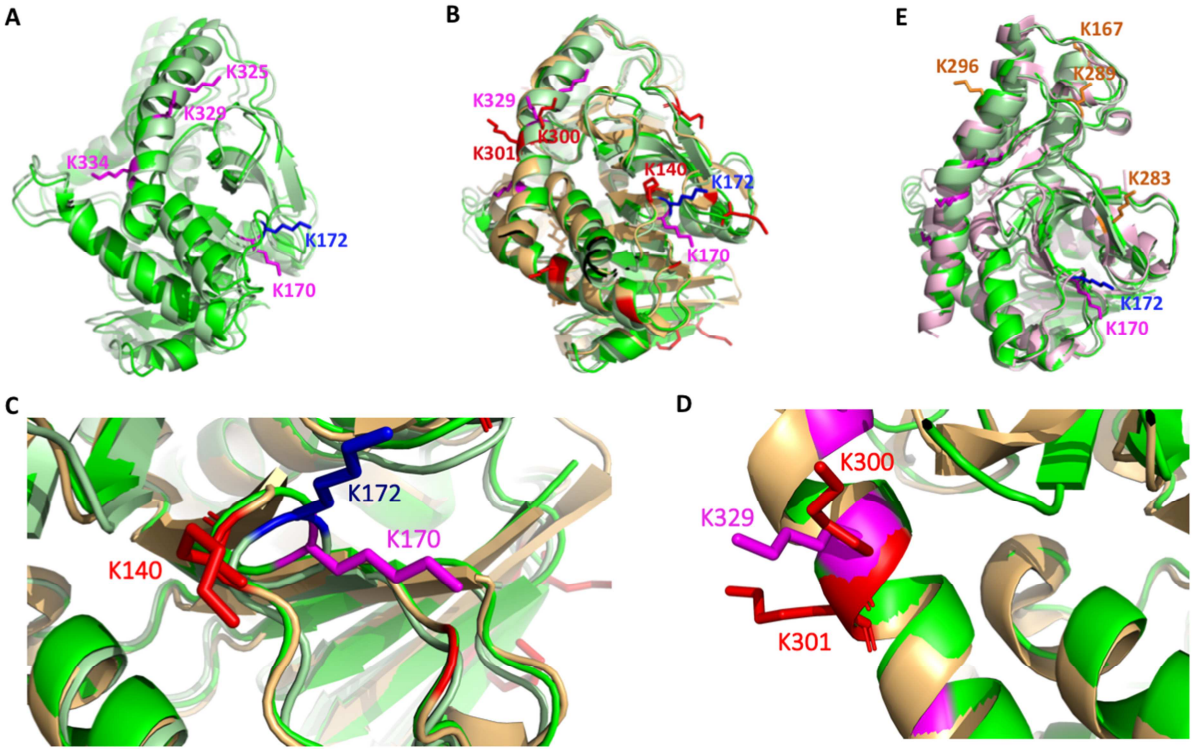

Figure 6. Superposition analysis of MDH monomeric structures. A. Structures of *A. thaliana* (bright green-magenta) and *P. patens* (dark green-blue) mMDH1. **B**. Structures of *A. thaliana* and *P. patens* mMDH1, and *E. coli* MDH (gold-red; PDB ID:1EMD). **C.** Zoom in of the region containing K170 in *A. thaliana* (bright green-magenta) mMDH1, K172 in *P. patens* (dark green-blue) mMDH1 and K140 in *E. coli* (gold-red) MDH. **D.** Zoom in of the region containing K329 in *A. thaliana* (bright green-magenta) mMDH1 and K300 in *E. coli* (gold-red) MDH. **E.** *A. thaliana* and *P. patens* mMDH1, and human MDH2 (rose-brown; PDB ID: 2DFD). The acetylated lysine residues are shown in magenta for *A. thaliana* mMDH1, blue for *P. patens* mMDH1 red for *E. coli* MDH, and brown for human MDH2. For simplicity not all lysines found to be acetylated in *E. coli* are numbered.

Discussion

Lysine acetylation in mitochondrial proteins of evolutionary distant species

Acetylation of lysine residues is a particularly abundant posttranslational modification of mitochondrial and plastid proteomes (Lombard et al., 2007; König et al., 2014; Smith-Hammond et al., 2014; Hartl et al., 2017). Here, we detected 638 lysine acetylation sites in *P. patens* gametophores. Since lysine acetylation is a highly dynamic modification and its occurrence depends on the metabolic status of the organism (Meyer et al., 2018), the acetylation pattern may differ under different growth conditions. However, we aimed at considering analogous tissues for the comparison between *A. thaliana* and *P. patens*. Mitochondrial proteins were particularly overrepresented amongst lysine acetylated proteins detected, even more than in recent whole tissue acetylome studies of *A. thaliana* (Hartl et al. 2017, Uhrig et al. 2019). The number of 84 mitochondrial proteins identified here from whole

tissues is overall in line with 120 lysine-acetylated proteins that were detected in isolated Arabidopsis mitochondria of seedlings (König et al., 2014). Due to the lack of evidence for a mitochondrial acetyltransferase in most model organisms, it is anticipated that mitochondrial protein acetylation likely occurs non-enzymatically between specific lysine residues of particularly high reactivity and acetyl-CoA. The specific steady-state lysine acetylation pattern is likely set by enzymatically controlled de-acetylation, as carried out by sirtuine proteins (Lombard et al., 2007; König et al., 2014; Anderson et al., 2017). Mitochondrial hyperacetylation strongly affects respiration rates and cellular metabolism (Hebert et al., 2013; König et al., 2014). In general, lysine acetylation removes the positive charge from the lysine side chains of proteins and increases their hydrophobicity. However, similar to phosphorylation, lysine acetylation can affect protein function in various ways, as such that it can cause an activation as well as inhibition of enzymes for example, depending on the function of the particular lysine residue within the protein structure. Although, the identities of the acetylated mitochondrial protein targets are conserved between angiosperm species, the location of the particular lysine acetylation sites within the protein often differ (Finkemeier et al., 2011; Hosp et al., 2017). Our study shows that this is true across land plant phylogeny, since lysines, which were detected to be acetylated in one orthologous protein of the distant species *A. thaliana* and *P. patens,* were typically conserved in the orthologs of other species (Supplementary Table 4). However, even in the TCA cycle or PDC proteins, which showed high acetylation in both *P. patens* and *A. thaliana* (up to 5 acetylated lysines), only two detected acetylation sites were shared in total between the orthologs of the two species. A reason for the limited number of shared acetylated lysine residues detected might be the pronounced dynamics in lysine (de-)acetylation. The enzymes of the TCA cycle are known to be regulated by reversible acetylation in bacterial and mammalian cells, in dependence on the nutritional status as well as on the circadian clock (Wang et al., 2010; Masri et al., 2013; Meyer et al., 2018). While caloric restrictions generally lead to the deacetylation, nutrition with sugars (but not with high fat diet) leads to a strong increase in mitochondrial acetylation including all TCA cycle enzymes (Meyer et al., 2018). Acetylated lysines detected in different (even distant) species under diverse conditions might pinpoint those PTMs with particular metabolic or enzymatic relevance.

Lysine residues corresponding to K170 in *A. thaliana* mMDH1, for which acetylation led to a change in the enzyme activity, were found acetylated in three other species and also under different conditions, and were therefore best conserved. The same was observed for site K172

of MDH1 of *P. patens*. The corresponding lysine residues were also found acetylated in three angiosperm species. Likely the correlation between conservation of lysine acetylation sites and their functional significance can be used to predict a regulatory role of the lysine residues. Increasing the number of assessed lysine sites will allow to define if this observation can be generalized.

Acetylation of lysines within a conserved hotspot modulates plant MDH activity

In addition to the identification of acetylation of *E. coli* MDH and human mMDH2 (Venkat et al., 2017), recent proteomic studies report acetylation of plant mMDH proteins, albeit in different locations (Supplementary Table 5). To understand the potential functional significance of mMDH acetylation, which is the prerequisite for any regulatory role, we devised an empirical analysis of the enzyme characteristics.

Our analysis of the kinetic properties of plant mMDH1 in the OAA reduction direction indicated that lysine acetylation of K172 in *P. patens* and K170 in *A. thaliana* have opposite effects on the activities of the enzyme in both species. The turnover number of the *P. patens* mMDH1 carrying the acetylation at K172 is increased by 101% of the wild-type value. Thus, acetylation at K172 gives rise to a much effective enzyme, as it enables mMDH1 to convert OAA into pyruvate with a doubled rate compared with the non-modified protein. In contrast to this, the turnover number of *A. thaliana* mMDH1 acetylated at K170 is decreased to 37% of the non-acetylated form. Thus, the incorporation of an acetyl group at K170 in *A. thaliana* mMDH1 gives rise to a less effective enzyme that converts OAA into pyruvate with just above a third of the rate compared with the non-modified protein. A recent analysis of the protein composition of an individual average plant mitochondrion from cultured heterotrophic *A. thaliana* cells indicated that mMDH1 is highly abundant with about 13.190 copies per mitochondrion (Fuchs et al., 2020). Adding the *in vitro* activity changes measured here to this model a single mitochondrion without acetylation at the mMDH1 K170 site would have the capacity to turn over 7.2 Mio molecules of OAA per second, acetylation at K170 would reduce this conversion capacity to 2.7 Mio molecules per second. Since the adjustment is fully reversible and does not require protein synthesis and/or turnover it may plausibly represent an effective mechanism to module flux through central carbon metabolism. If and under which conditions exactly such modulation is relevant *in vivo* remains to be investigated in the future.

We found that the turnover number of *A. thaliana* wild-type mMDH1 is twice as high as that of *P. patens* wild-type mMDH1 (Fig. 4C), most likely reflecting an evolutive adjustment to the cellular metabolic necessities of each plant species. Interestingly, the opposite effects of acetylation of the lysine residues in both enzymes change the turnover numbers of the acetylated proteins to values similar to those found in the wild-type enzyme of the other species analysed: the turnover number of *P. patens* mMDH1 acetylated in K172 has a similar value to that of *A. thaliana* wild-type mMDH1 and *A. thaliana* mMDH1 acetylated in K170 has a similar turnover number value to that of *P. patens* wild-type mMDH1. These observations suggest that changes on the turnover number induced by acetylation of plant mMDH1 can occur between minimal and maximal values that are set by the structure and catalytic mechanism of the plant enzyme. Although the precise molecular reason for the changes in the turnover number are still to be determined it is interesting to note that amino acid 173 in *P. patens* mMDH1 (corresponding to K170 in *A. thaliana* mMDH1) is an arginine, which has similar properties as a permanent non-acetylated lysine (Kamieniarz and Schneider, 2009). Considering that the presence of an acetyl-lysine at position 170 of *A. thaliana* mMDH1 decreases the turnover number of the enzyme, the presence of an arginine in *P. patens* mMDH1 at the same position suggests that the *P. patens* wild-type enzyme is adapted to avoid a further reduction of its enzymatic activity. This interpretation correlates with the lower k_{cat} value we measured for the *P. patens* wild-type mMDH1 in comparison to that of the *A. thaliana* wild-type enzyme (Fig. 4C).

Interestingly, the lysine residues that influence the enzymatic activity of *A. thaliana* and *P. patens* mMDH1 in an acetylation-dependent manner are conserved in plants and were empirically found to be acetylated in several different species. Interestingly, in no case were the residues observed acetylated simultaneously. The fact that K169 and K170 were found to be independently acetylated in different organs (leaves and embryos) of rice may indicate the need of fine-tuning the enzyme activity to specific metabolic necessities of the organs.

Acetylation of *E. coli* MDH at K140, which is located next to *A. thaliana* K170 and *P. patens* K172, was shown to increase the enzymatic activity (by 3.4-fold) as assayed by malate oxidation (Venkat et al., 2017). In the same reaction direction, the *E. coli* enzyme is also activated by acetylation of K99 (by 2.3-fold) and the human mMDH2 increases its enzymatic activity (by 3.9-fold) by acetylation at K307 (Venkat et al., 2017). The impact of acetylation on the reduction of OAA to malate was not reported in those studies. It is interesting that in all cases analysed to date (our work and Venkat et al. (2017)), acetylation modifies the

turnover number of MDH without modifications of the affinity for the substrates, suggesting that this PTM may influences MDH activity through a common molecular mechanism.

Taken together, acetylation of lysine residues corresponding to K169 and K170 of *A. thaliana* mMDH1 impacts on the activity of the enzyme in different species. Our analysis of the modelled protein structures indicates that the critical lysine residues are not near the catalytic site or in the dimer or tetramer interfaces. The precise molecular mechanism of how acetylation impacts on the catalytic properties of the enzyme remains to be resolved, but the induction of a conformational change that reaches across the protein structure appears particularly likely. Consistent with this interpretation, we observed that *P. patens* mMDH1 acetylated at K172 shows a slightly enhanced mobility of both active oligomeric states on native PAGE as compared to the non-acetylated version.

Potential consequences of mMDH lysine acetylation for plant metabolism

Our results indicate that acetylation of *A. thaliana* mMDH1 at K170 reduces the rate of the reaction in the OAA reduction direction. Under conditions of high NAD^+/NADH ratio in the matrix, the activity of mMDH in the OAA reduction needs to be limited to avoid further removal of reductant from the matrix and constraints on mitochondrial ATP production in turn (Fig. 1). On the other hand, acetylation of *P. patens* mMDH1 at K172 increases the capacity – and potentially the rate – of OAA consumption under metabolic conditions that demand a high rate of matrix NAD^+ provision and less of ATP, e.g. during photorespiratory conditions (Fig. 1). In *E. coli* the activity of MDH in the malate oxidation direction and the acetylation grade of the enzyme increase with increasing glucose concentrations (Venkat et al., 2017), suggesting an activation of the enzyme to provide sufficient capacity for enhanced flux through the TCA-cycle in its circular mode. Interestingly, bacteria grown on citrate as carbon source showed lower acetylation of MDH as compared to growth in glucose, which favors the OAA reduction reaction of MDH (Wang et al., 2010; Mall et al., 2018).

The lysine residues found to be acetylated in mMDH1 of *A. thaliana* and *P. patens* most likely represent only a small proportion of the mMDH1 lysine sites that can be acetylated *in vivo*. As PTMs can be strictly dependent on the exact conditions, other lysine residues may also be acetylated in other tissues, different growth conditions, or different times of the day. More systematic analyses will be required in the future for their identification. Nevertheless, as in the case of other PTMs, not all acetylated lysines necessarily possess regulatory

function, as we here observed for the acetylation of K325, K329, and K334 of *A. thaliana* mMDH1, at least for the specific readout of the OAA reduction (Fig. 4C). Alternatively, these modifications may influence malate oxidation, i.e. the opposite direction of the reaction, or interactions with other proteins or factors that are not present in the *in vitro* setting devised here. Indeed, *in vivo* interactions between several mitochondrial proteins that were found to be acetylated in this study where recently reported in *A. thaliana in vivo* raising the possibility of further regulatory functions, e.g. by modulating metabolic channeling (Zhang et al., 2017; Zhang et al., 2018).

Methods

Physcomitrium patens cultivation conditions

P. patens (Hedw.) Bruch & Schimp. strain Gransden (Rensing et al., 2008) gametophores were cultivated on modified Knop medium plates (KH_2PO_4 (250 mg L^{-1}), KCl (250 mg L^{-1}), $MgSO_4$ x $7H_20$ (250 mg L^{-1}), $Ca(NO_3)_2$ x $4H_2O$ (1000 mg L^{-1}), $FeSO_4$ x $7H_2O$ (12.5 mg L^{-1}), $CuSO_4$ (0.22 µM), $ZnSO_4$ (0.19 µM), H_3BO_3 (10 µM), Na_2MoO_4 (0.1 µM), $MnCl_2$ (2 µM), $CoCl_2$ (0.23 µM) and KI (0.17 µM), pH = 5.8, 1% [w/v] agar; Rüdinger et al., 2011) at 21°C and 10 h light/14 h darkness using neon tubes Osram HO 39W/865 Lumilux Cool Daylight at a light intensity of 65 µmol m^{-2} s^{-1}. Single gametophores were transferred onto plates three weeks prior to harvest.

Trypsin digestion, immuno-enrichment of lysine-acetylated peptides and LC-MS/MS data acquisition

The lysine acetylome analysis was performed as described in detail in Lassowskat et al. (2017). Briefly, proteins were extracted from three independent replicates (including 5-6 gametophores/plate and 9-15 plates per replicate). Protein extracts were alkylated and digested with MS-grade trypsin. Peptides were desalted and enriched for lysine-acetylated proteins by immuno-purification. Total peptide samples and the immuno-enriched fractions were then analyzed via LC-MS/MS using an EASY-nLC 1200 (Thermo Fisher) coupled to a Q Exactive HF mass spectrometer (Thermo Fisher). Peptides were separated on 20 cm frit-less silica emitters (New Objective, 0.75 µm inner diameter), packed in-house with reversed-phase ReproSil-Pur C18 AQ 1.9 µm resin (Dr. Maisch). The column was kept at 50°C in a column oven throughout the run. The following parameters were used for acetylome analysis:

Peptides were eluted for 78 min using a segmented linear gradient of 0 to 98% solvent B (solvent A 0% ACN, 0.1% FA; solvent B 80% ACN, 0.1% FA) at a flow-rate of 250 nL/min. Mass spectra were acquired in data-dependent acquisition mode with a Top12 method. MS spectra were acquired in the Orbitrap analyzer with a mass range of 300–1759 m/z at a resolution of 120000 FWHM, maximum IT of 55 ms and a target value of 3×10^6 ions. Precursors were selected with an isolation window of 1.2 m/z. HCD fragmentation was performed at a normalized collision energy of 25. MS/MS spectra were acquired with a target value of 5×10^4 ions at a resolution of 15000 FWHM, maximum IT of 150 ms and a fixed first mass of m/z 100. Peptides with a charge of +1, greater than 6, or with unassigned charge state were excluded from fragmentation for MS2, and dynamic exclusion for 30 s prevented repeated selection of precursors.

MS data analysis

Raw data were processed using the MaxQuant software V1.6.17 (http://www.maxquant.org/) (Cox and Mann, 2008). MS/MS spectra were searched with the Andromeda engine against the cosmoss_V3.3 database. Sequences of 248 common contaminant proteins and decoy sequences were automatically added during the search. Trypsin specificity was required and a maximum of four missed cleavages were allowed. Minimal peptide length was set to seven amino acids. Carbamidomethylation of cysteine residues was set as fixed, oxidation of methionine and protein N-terminal acetylation, acetylation of lysines as variable modifications. Light and medium dimethylation of lysines and peptide N-termini were set as labels. Peptide-spectrum-matches and proteins were retained if they were below a false discovery rate of 1%, modified peptides were additionally filtered for a score ≥ 35 and a delta score of ≥ 6 to remove low quality identifications. Match between runs and requantify options were enabled. For acetylome analyses reverse hits and contaminants were removed. Acetylation sites were filtered for a localization probability of ≥ 0.75.

Functional classification and prediction of subcellular localization

Proteins were functional annotated based on the *P. patens* V3.3 database (Lang et al., 2018); cosmoss_V3.3.release.pep.fasta, Supplementary Data 1). Localization was inferred from the experimental dataset by Müller et al. (Müller et al., 2014) and the GO_CC annotation provided in Lang et al. (2018).

Comparison of acetylated lysines of putative mitochondrial orthologs between *A. thaliana* and *P. patens*

Sequences of the 120 acetylated *A. thaliana* proteins identified in König et al. (König et al., 2014) were obtained from Tair (https://www.arabidopsis.org/tools/bulk/sequences/index.jsp) and sequences of those *P. patens* proteins that were acetylated and classified were obtained from Peatmoss (https://peatmoss.online.uni-marburg.de/ppatens_db/pp_search_input.php) (Fernandez-Pozo et al., 2020). Amino acid sequences of both species were combined and orthologous groups with sequence similarity higher than 40 % were clustered using the multiple alignment program MAFFT Version 7 with default settings (https://mafft.cbrc.jp/alignment/server/). *P. patens* and *A. thaliana* proteins were aligned again with Muscle (Edgar, 2004) using the Mega 7 software (Kumar et al., 2016). In total 22 clusters of *P. patens* and *A. thaliana* protein homologs were identified. In each cluster different numbers of paralogous proteins of each species were included. Acetylation sites of each single protein were compared with each other and acetylation sites shared between one of the paralogous proteins of *A. thaliana* and *P. patens* were listed and positions extracted from the original alignment (Table 1, Supplementary Table 4).

Phylogenetic analysis, comparison of sequence conservation and lysine acetylation patterns of mMDHs of different plant species

Published acetylome datasets were inspected for the presence of the mitochondrial malate dehydrogenase. In total 18 datasets for 11 different flowering plants were included in the analysis (Supplementary Table 5). For seven flowering plant species lysine acetylation of mMDH proteins was detected. Plant tissues or organs, in which these lysine acetylated mMDHs were detected, are given in Supplementary Table 5. Putative mMDH orthologs of these species were identified by Basic Local Alignment Tool (BLAST) searches using the *A. thaliana* mMDH1 protein sequence as query against nonredundant protein database (BLASTP) and against translated nucleotide database (TBLASTN) (Altschul et al., 1990) of different sources. Sequence data of the selected angiosperm species *C. sinensis*, *V. vinifera*, *O. sativa, B. distachyon, F. ananass* and the green algae *C. reinhardii* were deposited at NCBI (www.ncbi.nlm.nih.gov) and sequence data of *P. patens* and *M. polymorpha* are deposited at Phytozome v12.0 (https://phytozome.jgi.doe.gov/pz/portal.html). For putative mMDH orthologs of Azolla and Salvinia, sequences are available in the Fernbase (www.fernbase.org). For *P. sativum* the URGI database was used as sequence source

(Kreplak et al., 2019). The *Anthoceros* sequences were retrieved from the recently published *A. agrestis*, Bonn v1 strain genome v1.1 (Li et al., 2020). Best 2-10 hits were downloaded for each species and were aligned in the MEGA alignment explorer with the MUSCLE tool (Tamura et al., 2015; Kumar et al., 2016) followed by manual adjustment.

Amino acid sequence alignment was used to calculate a Neighbor joining phylogeny with 1000 bootstraps (Poisson model, gamma distributed, partial deletion with cut off 90 %) including the peroxisomal (AT2G22780), plastidial (AT3G47520) and mitochondrial *A. thaliana* mMDH proteins. With a reduced dataset including all MDH proteins of the identified cluster, mitochondrial, glyoxysomal/peroxisomal and plastid MDHs of *P. patens* and *A. thaliana* and the MDH of *E. coli* and the mMDH2 of human, we constructed a Maximum Likelihood phylogram using IQ-tree webserver (Trifinopoulos et al., 2016) (Supplementary Fig. 1). We applied the LG+G4 model for sequence evolution as the best fitting model identified by ModelFinder (Kalyaanamoorthy et al., 2017). We determined the confidence of each node from 1,000 bootstrap replicates with ultrafast bootstrap approximation "UFBoot" (Hoang et al., 2018). In parallel we calculated a Neighbor joining phylogeny with same settings as described above (Supplementary Fig. 1). Sequences of mMDH proteins identified to be acetylated were aligned and conservation was displayed using the GeneDoc software (https://genedoc.software.informer.com/2.7/).

Cloning of *A. thaliana* mMDH1 into the expression vector

The cDNA encoding the mMDH1 mature protein (without signal peptide) from *A. thaliana* (Hüdig et al., 2015) was introduced in pCDF PylT-1 vector (SmR; *T7* promoter; *T7* terminator) (Neumann et al., 2009). This vector allows the expression of proteins fused to an N-terminal His tag for purification by Ni-NTA affinity chromatography. The mMDH cassette was obtained by PCR using primers mmdh1_GibFw and mmdh1_GibRv and cloned by Gibson assembly. The sequence of the resulting plasmid was verified by sequencing. The pCDFmdh1 vector was used as template for site directed mutagenesis by PCR, to change specific lysine codons to the amber codon, using the primers listed in Supplementary Table 6. The following constructs were generated: pCDFmdh1amb170, pCDFmdh1amb325, pCDFmdh1amb329, pCDFmdh1amb334. The incorporation of the desired nucleotide changes was confirmed by sequencing (Macrogen).

Cloning of *P. patens* mMDH1 into the expression vector

The coding sequence of mMDH1 (without signal peptide) of *P. patens* Gransden (gene Pp1s201_6V6.1) (Lang et al., 2018) was amplified with primers MfeI_PpMDH1_f and KpnI_PpMDH1_r (Supplementary Table 6). The mMDH1 version with the amber codon for amino acid position 172 was generated by overlap extension PCR with internal primers (PpMDH1_KStop_f and PpMDH1_KStop_r, Supplementary Table 6). The fragments were introduced into the pCDF PylT-1 vector (SmR; *T7* promoter; *T7* terminator) between restriction sites *MfeI and KpnI* (SmR; *T7* promoter; *T7* terminator) (Neumann et al., 2009) to generate N-terminally His-tagged mMDH1. The incorporation of the desired nucleotide changes was confirmed by sequencing (Macrogen).

Expression and purification of acetylated mMDHs

All pCDF PylT expression constructs carrying the mMDH1 versions with an amber codon instead of the codon for the lysine to be acetylated and those carrying the corresponding wild-type mMDH1 were transformed into *E. coli* Rosetta2 (DE3). Plasmid pBK-AcKRS3 (carrying the acetyl-lysyl-tRNA synthetase (AckRS); (Neumann et al., 2008)) was co-transformed with the pCDF PylT plasmids. For heterologous protein production, transformed cells were grown in 400 ml LB medium in the presence of the appropriate antibiotic in each case at 37°C and 16 *g* to an OD600 of 0.4-0.6. The growth medium was supplemented with 10 mM N^{ϵ}-acetyl-lysine and 20 mM nicotinamide 30 min before induction. To induce the expression of the heterologous protein, 1 mM IPTG was added to the culture and the cells were incubated for 20 h at 30°C and 16 *g*. The cellular culture was harvested at 6,000 *g* for 15 min, and pellets were stored at -20°C until use.

For protein extraction, pellets were thawed on ice, resuspended in 20 mM Tris-HCl (pH 8.0) containing 500 mM NaCl, 5 mM imidazole, 1 mM phenylmethylsulfonyl fluoride and a spatula-tip of lysozyme, sonicated and centrifuged at 14,000 *g* for 20 min at 4°C. The supernatant was used for protein purification by gravity-flow immobilized metal ion chromatography on nickel-nitrilotriacetic acid agarose (Ni-NTA Agarose, ThermoFisher). The column was pre-equilibrated with 20 mM Tris-HCl buffer containing 500 mM NaCl and 5 mM imidazole. After loading of the supernatant, the columns were washed in four steps with 500 mM NaCl in 20 mM Tris-HCl (pH 8.0) containing increasing concentrations of imidazole (5, 40 and 60 mM). Protein elution was performed in four steps of 500 µl of 20

mM Tris-HCl, 500 mM NaCl and 200 mM imidazole. Finally, Vivaspin® 10K columns (Satorius, Germany) were used for protein concentration and buffer exchanging (HEPES 50 mM, pH 7.4). The isolated recombinant proteins were analysed by SDS-PAGE and LC-MS/MS (see above) to verify integrity and purity. Protein concentration was determined by Amido black assay (Dieckmann-Schuppert and Schnittler, 1997).

Kinetic characterization of acetylated mMDH1

MDH activity assays were carried on in a Synergy HT Biotek Plate Reader system at 25°C following the oxidation of NADH at 340 nm (ε= 6.2 cm^{-1} mM^{-1}). The assay medium contained 50 mM Hepes pH 7.5, 10 mM $MgCl_2$, 5 mM NADH and variable concentrations of OAA in the range 0.01 to 4 mM.

The reactions were started by the addition of the substrate. The kinetic constants were calculated with a minimum of three different enzyme batches each in at least triplicate determinations and adjusted to non-linear regression (Sigma Plot).

Gel electrophoresis

SDS-PAGE was performed using 14% (w/v) polyacrylamide gels according to (Laemmli, 1970) and the molecular weight markers were Spectra Multicolor Broad Range Protein Ladder (ThermoFisher Scientific). Proteins were visualized by staining with Coomassie Brilliant Blue. Purified enzymes were analyzed on a non-denaturing 12% (w/v) polyacrylamide gel. In-gel mMDH activity assays were performed by incubating the gels in the dark at room temperature in a reaction buffer containing 50 mM K_2PO_4 (pH 7.4), 5 mM malate, 0.2 mM NAD, 0.05% (w/v) NBT and 10 µM PMS as described in Hüdig et al. (2015).

Statistical analyses

Statistical analyses of the kinetic data were performed on data from at least three biological replicate samples. To verify the statistical differences, P values were determined using one-way ANOVA and Dunnett's test, and unpaired t-test.

Homology modelling of mMDH 3-D structures

The 3-D models of *E. coli* MDH (PDB code 1EMD) and *H. sapiens* MDH2 (PDB code 2DFD) structures were obtained from the RSCB Protein Data Bank (https://www.rcsb.org/). Both *A. thaliana* and *P. patens* mMDH1 models were obtained by using the phyre2 protein structure prediction server (http://www.sbg.bio.ic.ac.uk/~phyre2/html/page.cgi?id=index) with the corresponding amino acid sequence as input. The ligand molecules NAD^+ and citrate were manually fitted in by aligning the structure of the *H. sapiens* MDH2 (pdb code 2DFD) to the modelled structures of *A. thaliana* and *P. patens* mMDH1. Images of the models were prepared using PyMOL v.2.4.0 by Schrödinger (https://pymol.org/).

Acknowledgements

This work was enabled through the collaborative DFG research grant PAK918 (IF1655/3-1, MA2379/14-1, SCHA1953/3-1, SCHW1719/5-1) as part of the 'Plant Mitochondria in New Light' initiative and INST 211/744-1 FUGG for LC-MS/MS analyses. Work of MB in the group of VGM was funded by the StayConnected-Grant of the Heinrich Heine University Düsseldorf. The pBK PylS and pCDF PylT vectors were provided by Dr. J. Chin (University of Cambridge) under a non-commercial material transfer agreement to IF. We thank Astrid Höppner (HHU, Düsseldorf) for her help with the structural analysis.

REFERENCES

Allfrey VG, Faulkner R, Mirsky AE (1964) Acetylation and Methylation of Histones and Their Possible Role in the Regulation of RNA Synthesis. Proc Natl Acad Sci U S A **51:** 786-794

Altschul SF, Gish W, Miller W, Myers EW, Lipman DJ (1990) Basic local alignment search tool. J Mol Biol **215:** 403-410

Anderson KA, Madsen AS, Olsen CA, Hirschey MD (2017) Metabolic control by sirtuins and other enzymes that sense NAD^+, NADH, or their ratio. Biochim Biophys Acta Bioenerg **1858:** 991-998

Bovdilova A, Alexandre BM, Hoppner A, Matias Luis I, Alvarez CE, Bickel D, Gohlke H, Decker C, Nagel-Steger L, Alseekh S, Fernie AR, Drincovich MF, Abreu IA, Maurino VG (2019) Posttranslational modification of the NADP-malic enzyme involved in C4 photosynthesis fine-tunes the enzymatic activity during the day. Plant Cell **10.1105/tpc.19.00406**

Choudhary C, Weinert BT, Nishida Y, Verdin E, Mann M (2014) The growing landscape of lysine acetylation links metabolism and cell signalling. Nat Rev Mol Cell Biol **15:** 536-550

Cox J, Mann M (2008) MaxQuant enables high peptide identification rates, individualized p.p.b.-range mass accuracies and proteome-wide protein quantification. Nat Biotechnol **26:** 1367-1372

Dieckmann-Schuppert A, Schnittler HJ (1997) A simple assay for quantification of protein in tissue sections, cell cultures, and cell homogenates, and of protein immobilized on solid surfaces. Cell Tissue Res **288:** 119-126

Edgar RC (2004) MUSCLE: multiple sequence alignment with high accuracy and high throughput. Nucleic Acids Res **32:** 1792-1797

Fang X, Chen W, Zhao Y, Ruan S, Zhang H, Yan C, Jin L, Cao L, Zhu J, Ma H, Cheng Z (2015) Global analysis of lysine acetylation in strawberry leaves. Front Plant Sci **6:** 739

Fernandez-Pozo N, Haas FB, Meyberg R, Ullrich KK, Hiss M, Perroud PF, Hanke S, Kratz V, Powell AF, Vesty EF, Daum CG, Zane M, Lipzen A, Sreedasyam A, Grimwood J, Coates JC, Barry K, Schmutz J, Mueller LA, Rensing SA (2020) PEATmoss (Physcomitrella Expression Atlas Tool): a unified gene expression atlas for the model plant Physcomitrella patens. Plant J **102:** 165-177

Finkemeier I, Laxa M, Miguet L, Howden AJ, Sweetlove LJ (2011) Proteins of diverse function and subcellular location are lysine acetylated in Arabidopsis. Plant Physiol **155:** 1779-1790

Fuchs P, Rugen N, Carrie C, Elsässer M, Finkemeier I, Giese J, Hildebrandt TM, Kühn K, Maurino VG, Ruberti C, Schallenberg-Rüdinger M, Steinbeck J, Braun HP, Eubel H, Meyer EH, Müller-Schüssele SJ, Schwarzländer M (2020) Single organelle function and organization as estimated from Arabidopsis mitochondrial proteomics. Plant J **101:** 420-441

Gleason WB, Fu Z, Birktoft J, Banaszak L (1994) Refined crystal structure of mitochondrial malate dehydrogenase from porcine heart and the consensus structure for dicarboxylic acid oxidoreductases. Biochemistry **33:** 2078-2088

Group TAP (2009) An update of the Angiosperm Phylogeny Group classification for the orders and families of flowering plants: APG III. . Botanical Journal of the Linnean Society **161:** 105-121

Guan KL, Xiong Y (2011) Regulation of intermediary metabolism by protein acetylation. Trends Biochem Sci **36:** 108-116

Hanning I, Heldt HW (1993) On the Function of Mitochondrial Metabolism during Photosynthesis in Spinach (Spinacia oleracea L.) Leaves (Partitioning between Respiration and Export of Redox Equivalents and Precursors for Nitrate Assimilation Products). Plant Physiol **103:** 1147-1154

Hartl M, Fussl M, Boersema PJ, Jost JO, Kramer K, Bakirbas A, Sindlinger J, Plochinger M, Leister D, Uhrig G, Moorhead GB, Cox J, Salvucci ME, Schwarzer D, Mann M, Finkemeier I (2017) Lysine acetylome profiling uncovers novel histone deacetylase substrate proteins in Arabidopsis. Mol Syst Biol **13:** 949

He D, Wang Q, Li M, Damaris RN, Yi X, Cheng Z, Yang P (2016) Global Proteome Analyses of Lysine Acetylation and Succinylation Reveal the Widespread Involvement of both Modification in Metabolism in the Embryo of Germinating Rice Seed. J Proteome Res **15:** 879-890

Hebert AS, Dittenhafer-Reed KE, Yu W, Bailey DJ, Selen ES, Boersma MD, Carson JJ, Tonelli M, Balloon AJ, Higbee AJ, Westphall MS, Pagliarini DJ, Prolla TA, Assadi-Porter F, Roy S, Denu JM, Coon JJ (2013) Calorie restriction and SIRT3 trigger global reprogramming of the mitochondrial protein acetylome. Mol Cell **49:** 186-199

Hirschey MD, Shimazu T, Huang JY, Schwer B, Verdin E (2011) SIRT3 regulates mitochondrial protein acetylation and intermediary metabolism. Cold Spring Harb Symp Quant Biol **76:** 267-277

Hoang DT, Chernomor O, von Haeseler A, Minh BQ, Vinh LS (2018) UFBoot2: Improving the Ultrafast Bootstrap Approximation. Mol Biol Evol **35:** 518-522

Hosp F, Lassowskat I, Santoro V, De Vleesschauwer D, Fliegner D, Redestig H, Mann M, Christian S, Hannah MA, Finkemeier I (2017) Lysine acetylation in mitochondria: From inventory to function. Mitochondrion **33:** 58-71

Hüdig M, Maier A, Scherrers I, Seidel L, Jansen EE, Mettler-Altmann T, Engqvist MK, Maurino VG (2015) Plants Possess a Cyclic Mitochondrial Metabolic Pathway similar to the Mammalian Metabolic Repair Mechanism Involving Malate Dehydrogenase and l-2-Hydroxyglutarate Dehydrogenase. Plant Cell Physiol **56:** 1820-1830

Imai S, Armstrong CM, Kaeberlein M, Guarente L (2000) Transcriptional silencing and longevity protein Sir2 is an NAD-dependent histone deacetylase. Nature **403:** 795-800

Inuzuka H, Gao D, Finley LW, Yang W, Wan L, Fukushima H, Chin YR, Zhai B, Shaik S, Lau AW, Wang Z, Gygi SP, Nakayama K, Teruya-Feldstein J, Toker A, Haigis MC, Pandolfi PP, Wei W (2012) Acetylation-dependent regulation of Skp2 function. Cell **150:** 179-193

Jiang J, Gai Z, Wang Y, Fan K, Sun L, Wang H, Ding Z (2018) Comprehensive proteome analyses of lysine acetylation in tea leaves by sensing nitrogen nutrition. BMC Genomics **19:** 840

Journet EP, Neuburger M, Douce R (1981) Role of Glutamate-oxaloacetate Transaminase and Malate Dehydrogenase in the Regeneration of NAD for Glycine Oxidation by Spinach leaf Mitochondria. Plant Physiol **67:** 467-469

Kalyaanamoorthy S, Minh BQ, Wong TKF, von Haeseler A, Jermiin LS (2017) ModelFinder: fast model selection for accurate phylogenetic estimates. Nat Methods **14:** 587-589

Kamieniarz K, Schneider R (2009) Tools to tackle protein acetylation. Chem Biol **16:** 1027-1029

König AC, Hartl M, Boersema PJ, Mann M, Finkemeier I (2014) The mitochondrial lysine acetylome of Arabidopsis. Mitochondrion **19:** 252-260

König AC, Hartl M, Pham PA, Laxa M, Boersema PJ, Orwat A, Kalitventseva I, Plochinger M, Braun HP, Leister D, Mann M, Wachter A, Fernie AR, Finkemeier I (2014) The Arabidopsis class II sirtuin is a lysine deacetylase and interacts with mitochondrial energy metabolism. Plant Physiol **164:** 1401-1414

Kreplak J, Madoui MA, Capal P, Novak P, Labadie K, Aubert G, Bayer PE, Gali KK, Syme RA, Main D, Klein A, Berard A, Vrbova I, Fournier C, d'Agata L, Belser C, Berrabah W, Toegelova H, Milec Z, Vrana J, Lee H, Kougbeadjo A, Terezol M, Huneau C, Turo CJ, Mohellibi N, Neumann P, Falque M, Gallardo K, McGee R, Tar'an B, Bendahmane A, Aury JM, Batley J, Le Paslier MC, Ellis N, Warkentin TD, Coyne CJ, Salse J, Edwards D, Lichtenzveig J, Macas J, Dolezel J, Wincker P, Burstin J (2019) A reference genome for pea provides insight into legume genome evolution. Nat Genet **51:** 1411-1422

Kumar S, Stecher G, Tamura K (2016) MEGA7: Molecular Evolutionary Genetics Analysis Version 7.0 for Bigger Datasets. Mol Biol Evol **33:** 1870-1874

Laemmli UK (1970) Cleavage of structural proteins during the assembly of the head of bacteriophage T4. Nature **227:** 680-685

Lang D, Ullrich KK, Murat F, Fuchs J, Jenkins J, Haas FB, Piednoel M, Gundlach H, Van Bel M, Meyberg R, Vives C, Morata J, Symeonidi A, Hiss M, Muchero W, Kamisugi Y, Saleh O, Blanc G, Decker EL, van Gessel N, Grimwood J, Hayes RD, Graham SW, Gunter LE, McDaniel SF, Hoernstein SNW, Larsson A, Li FW, Perroud PF, Phillips J, Ranjan P, Rokshar DS, Rothfels CJ, Schneider L, Shu S, Stevenson DW, Thummler F, Tillich M, Villarreal Aguilar JC, Widiez T, Wong GK, Wymore A, Zhang Y, Zimmer AD, Quatrano RS, Mayer KFX, Goodstein D, Casacuberta JM, Vandepoele K, Reski R, Cuming AC, Tuskan GA, Maumus F, Salse J, Schmutz J, Rensing SA (2018) The Physcomitrella patens chromosome-scale assembly reveals moss genome structure and evolution. Plant J **93:** 515-533

Lassowskat I, Hartl M, Hosp F, Boersema PJ, Mann M, Finkemeier I (2017) Dimethyl-labeling based quantification of the lysine acetylome and proteome of plants. Methods Mol Biol, photorespiration, AFeaE (ed), **1653:** 65–81

Li FW, Nishiyama T, Waller M, Frangedakis E, Keller J, Li Z, Fernandez-Pozo N, Barker MS, Bennett T, Blazquez MA, Cheng S, Cuming AC, de Vries J, de Vries S, Delaux PM, Diop IS, Harrison CJ, Hauser D, Hernandez-Garcia J, Kirbis A, Meeks JC, Monte I, Mutte SK, Neubauer A, Quandt D, Robison T, Shimamura M, Rensing SA, Villarreal JC, Weijers D, Wicke S, Wong GK, Sakakibara K, Szovenyi P (2020) Anthoceros genomes illuminate the origin of land plants and the unique biology of hornworts. Nat Plants **6:** 259-272

Lin H, Su X, He B (2012) Protein lysine acylation and cysteine succination by intermediates of energy metabolism. ACS Chem Biol **7:** 947-960

Lombard DB, Alt FW, Cheng HL, Bunkenborg J, Streeper RS, Mostoslavsky R, Kim J, Yancopoulos G, Valenzuela D, Murphy A, Yang Y, Chen Y, Hirschey MD, Bronson RT, Haigis M, Guarente LP, Farese RV, Jr., Weissman S, Verdin E, Schwer B (2007) Mammalian Sir2 homolog SIRT3 regulates global mitochondrial lysine acetylation. Mol Cell Biol **27:** 8807-8814

Lu Y, Xu Q, Liu Y, Yu Y, Cheng ZY, Zhao Y, Zhou DX (2018) Dynamics and functional interplay of histone lysine butyrylation, crotonylation, and acetylation in rice under starvation and submergence. Genome Biol **19:** 144

Mall A, Sobotta J, Huber C, Tschirner C, Kowarschik S, Bacnik K, Mergelsberg M, Boll M, Hugler M, Eisenreich W, Berg IA (2018) Reversibility of citrate synthase allows autotrophic growth of a thermophilic bacterium. Science **359:** 563-567

Masri S, Patel VR, Eckel-Mahan KL, Peleg S, Forne I, Ladurner AG, Baldi P, Imhof A, Sassone-Corsi P (2013) Circadian acetylome reveals regulation of mitochondrial metabolic pathways. Proc Natl Acad Sci U S A **110:** 3339-3344

Matsuzaki H, Daitoku H, Hatta M, Aoyama H, Yoshimochi K, Fukamizu A (2005) Acetylation of Foxo1 alters its DNA-binding ability and sensitivity to phosphorylation. Proc Natl Acad Sci U S A **102:** 11278-11283

Maurino VG, Engqvist MK (2015) 2-Hydroxy Acids in Plant Metabolism. Arabidopsis Book **13:** e0182

Melo-Braga MN, Verano-Braga T, Leon IR, Antonacci D, Nogueira FC, Thelen JJ, Larsen MR, Palmisano G (2012) Modulation of protein phosphorylation, N-glycosylation and Lys-acetylation in grape (Vitis vinifera) mesocarp and exocarp owing to Lobesia botrana infection. Mol Cell Proteomics **11:** 945-956

Meyer JG, Softic S, Basisty N, Rardin MJ, Verdin E, Gibson BW, Ilkayeva O, Newgard CB, Kahn CR, Schilling B (2018) Temporal dynamics of liver mitochondrial protein acetylation and succinylation and metabolites due to high fat diet and/or excess glucose or fructose. PLoS One **13:** e0208973

Mo R, Yang MK, Chen Z, Cheng ZY, Yi XL, Li CY, He CL, Xiong Q, Chen H, Wang Q, Ge F (2015) Acetylome Analysis Reveals the Involvement of Lysine Acetylation in Photosynthesis and Carbon Metabolism in the Model Cyanobacterium Synechocystis sp PCC 6803. Journal of Proteome Research **14:** 1275-1286

Moller IM, Igamberdiev AU, Bykova NV, Finkemeier I, Rasmusson AG, Schwarzlander M (2020) Matrix Redox Physiology Governs the Regulation of Plant Mitochondrial Metabolism through Posttranslational Protein Modifications. Plant Cell **32:** 573-594

Müller SJ, Lang D, Hoernstein SN, Lang EG, Schuessele C, Schmidt A, Fluck M, Leisibach D, Niegl C, Zimmer AD, Schlosser A, Reski R (2014) Quantitative analysis of the mitochondrial and plastid proteomes of the moss Physcomitrella patens reveals protein macrocompartmentation and microcompartmentation. Plant Physiol **164:** 2081-2095

Murphey WH, Kitto GB, Everse J, Kaplan N (1967) Malate dehydrogenases. I. A survey of molecular size measured by gel filtration. Biochemistry **6:** 603-610

Neumann H, Hancock SM, Buning R, Routh A, Chapman L, Somers J, Owen-Hughes T, van Noort J, Rhodes D, Chin JW (2009) A method for genetically installing site-specific acetylation in recombinant histones defines the effects of H3 K56 acetylation. Mol Cell **36:** 153-163

Neumann H, Peak-Chew SY, Chin JW (2008) Genetically encoding N(epsilon)-acetyllysine in recombinant proteins. Nat Chem Biol **4:** 232-234

Noyes BE, Glatthaar BE, Garavelli JS, Bradshaw RA (1974) Structural and functional similarities between mitochondrial malate dehydrogenase and L-3-hydroxyacyl CoA dehydrogenase. Proc Natl Acad Sci U S A **71:** 1334-1338

Qiu YL, Li L, Wang B, Chen Z, Knoop V, Groth-Malonek M, Dombrovska O, Lee J, Kent L, Rest J, Estabrook GF, Hendry TA, Taylor DW, Testa CM, Ambros M, Crandall-Stotler B, Duff RJ, Stech M, Frey W, Quandt D, Davis CC (2006) The deepest divergences in land plants inferred from phylogenomic evidence. Proc Natl Acad Sci U S A **103:** 15511-15516

Rensing SA, Goffinet B, Meyberg R, Wu SZ, Bezanilla M (2020) The Moss Physcomitrium (Physcomitrella) patens: A Model Organism for Non-Seed Plants. Plant Cell **32:** 1361-1376

Rensing SA, Lang D, Zimmer AD, Terry A, Salamov A, Shapiro H, Nishiyama T, Perroud PF, Lindquist EA, Kamisugi Y, Tanahashi T, Sakakibara K, Fujita T, Oishi K, Shin IT, Kuroki Y, Toyoda A, Suzuki Y, Hashimoto S, Yamaguchi K, Sugano S, Kohara Y, Fujiyama A, Anterola A, Aoki S, Ashton N, Barbazuk WB, Barker E, Bennetzen JL, Blankenship R, Cho SH, Dutcher SK, Estelle M, Fawcett JA, Gundlach H, Hanada K, Heyl A, Hicks KA, Hughes J, Lohr M, Mayer K, Melkozernov A, Murata T, Nelson DR, Pils B, Prigge M, Reiss B,

Renner T, Rombauts S, Rushton PJ, Sanderfoot A, Schween G, Shiu SH, Stueber K, Theodoulou FL, Tu H, Van de Peer Y, Verrier PJ, Waters E, Wood A, Yang L, Cove D, Cuming AC, Hasebe M, Lucas S, Mishler BD, Reski R, Grigoriev IV, Quatrano RS, Boore JL (2008) The Physcomitrella genome reveals evolutionary insights into the conquest of land by plants. Science **319:** 64-69

Rüdinger M, Szövenyi P, Rensing SA, Knoop V (2011) Assigning DYW-type PPR proteins to RNA editing sites in the funariid mosses Physcomitrella patens and Funaria hygrometrica. Plant J **67:** 370–80.

Scheibe R (2004) Malate valves to balance cellular energy supply. Physiol Plant **120:** 21-26

Scheibe R, Backhausen JE, Emmerlich V, Holtgrefe S (2005) Strategies to maintain redox homeostasis during photosynthesis under changing conditions. J Exp Bot **56:** 1481-1489

Schilling B, Christensen D, Davis R, Sahu AK, Hu LI, Walker-Peddakotla A, Sorensen DJ, Zemaitaitis B, Gibson BW, Wolfe AJ (2015) Protein acetylation dynamics in response to carbon overflow in Escherichia coli. Mol Microbiol **98:** 847-863

Senkler J, Senkler M, Eubel H, Hildebrandt T, Lengwenus C, Schertl P, Schwarzlander M, Wagner S, Wittig I, Braun HP (2017) The mitochondrial complexome of Arabidopsis thaliana. Plant J **89:** 1079-1092

Shore JD, Chakrabarti SK (1976) Subunit dissociation of mitochondrial malate dehydrogenase. Biochemistry **15:** 875-879

Smith-Hammond CL, Hoyos E, Miernyk JA (2014) The pea seedling mitochondrial N(epsilon)-lysine acetylome. Mitochondrion **19 Pt B:** 154-165

Strotbek C, Krinninger S, Frank W (2013) The moss Physcomitrella patens: methods and tools from cultivation to targeted analysis of gene function. Int J Dev Biol **57:** 553-564

Sweetlove LJ, Beard KF, Nunes-Nesi A, Fernie AR, Ratcliffe RG (2010) Not just a circle: flux modes in the plant TCA cycle. Trends Plant Sci **15:** 462-470

Tamura Y, Ito A, Cresswell AG (2015) A systematic muscle model covering regions from the fast ramp stretches in the muscle fibres to the relatively slow stretches in the human triceps surae. Comput Methods Biomech Biomed Engin **18:** 97-106

Tomaz T, Bagard M, Pracharoenwattana I, Linden P, Lee CP, Carroll AJ, Stroher E, Smith SM, Gardestrom P, Millar AH (2010) Mitochondrial malate dehydrogenase lowers leaf respiration and alters photorespiration and plant growth in Arabidopsis. Plant Physiol **154:** 1143-1157

Trifinopoulos J, Nguyen LT, von Haeseler A, Minh BQ (2016) W-IQ-TREE: a fast online phylogenetic tool for maximum likelihood analysis. Nucleic Acids Res **44:** W232-235

Tronconi MA, Fahnenstich H, Gerrard Weehler MC, Andreo CS, Flugge UI, Drincovich MF, Maurino VG (2008) Arabidopsis NAD-malic enzyme functions as a homodimer and heterodimer and has a major impact on nocturnal metabolism. Plant Physiol **146:** 1540-1552

Tronconi MA, Hüdig M, Schranz ME, Maurino VG (2020) Independent recruitment of duplicated β-subunit-coding NAD-ME genes aided the evolution of C4 photosynthesis in Cleomaceae. Front. Plant Sci.

Venkat S, Gregory C, Sturges J, Gan Q, Fan C (2017) Studying the Lysine Acetylation of Malate Dehydrogenase. J Mol Biol **429:** 1396-1405

Ventura M, Mateo F, Serratosa J, Salaet I, Carujo S, Bachs O, Pujol MJ (2010) Nuclear translocation of glyceraldehyde-3-phosphate dehydrogenase is regulated by acetylation. Int J Biochem Cell Biol **42:** 1672-1680

Wang Q, Zhang Y, Yang C, Xiong H, Lin Y, Yao J, Li H, Xie L, Zhao W, Yao Y, Ning ZB, Zeng R, Xiong Y, Guan KL, Zhao S, Zhao GP (2010) Acetylation of metabolic enzymes coordinates carbon source utilization and metabolic flux. Science **327:** 1004-1007

Weinert BT, Wagner SA, Horn H, Henriksen P, Liu WR, Olsen JV, Jensen LJ, Choudhary C (2011) Proteome-wide mapping of the Drosophila acetylome demonstrates a high degree of conservation of lysine acetylation. Sci Signal **4:** ra48

Xu H, Zhang J, Zeng J, Jiang L, Liu E, Peng C, He Z, Peng X (2009) Inducible antisense suppression of glycolate oxidase reveals its strong regulation over photosynthesis in rice. J Exp Bot **60:** 1799-1809

Yang XJ, Seto E (2008) Lysine acetylation: codified crosstalk with other posttranslational modifications. Mol Cell **31:** 449-461

Yoshida K, Hisabori T (2016) Adenine nucleotide-dependent and redox-independent control of mitochondrial malate dehydrogenase activity in Arabidopsis thaliana. Biochim Biophys Acta **1857:** 810-818

Zhang Y, Beard KFM, Swart C, Bergmann S, Krahnert I, Nikoloski Z, Graf A, Ratcliffe RG, Sweetlove LJ, Fernie AR, Obata T (2017) Protein-protein interactions and metabolite channelling in the plant tricarboxylic acid cycle. Nat Commun **8:** 15212

Zhang Y, Swart C, Alseekh S, Scossa F, Jiang L, Obata T, Graf A, Fernie AR (2018) The Extra-Pathway Interactome of the TCA Cycle: Expected and Unexpected Metabolic Interactions. Plant Physiol **177:** 966-979

Zhao S, Xu W, Jiang W, Yu W, Lin Y, Zhang T, Yao J, Zhou L, Zeng Y, Li H, Li Y, Shi J, An W, Hancock SM, He F, Qin L, Chin J, Yang P, Chen X, Lei Q, Xiong Y, Guan KL (2010) Regulation of cellular metabolism by protein lysine acetylation. Science **327:** 1000-1004

Zhen S, Deng X, Wang J, Zhu G, Cao H, Yuan L, Yan Y (2016) First Comprehensive Proteome Analyses of Lysine Acetylation and Succinylation in Seedling Leaves of Brachypodium distachyon L. Sci Rep **6:** 31576

Supplementary Figure 1

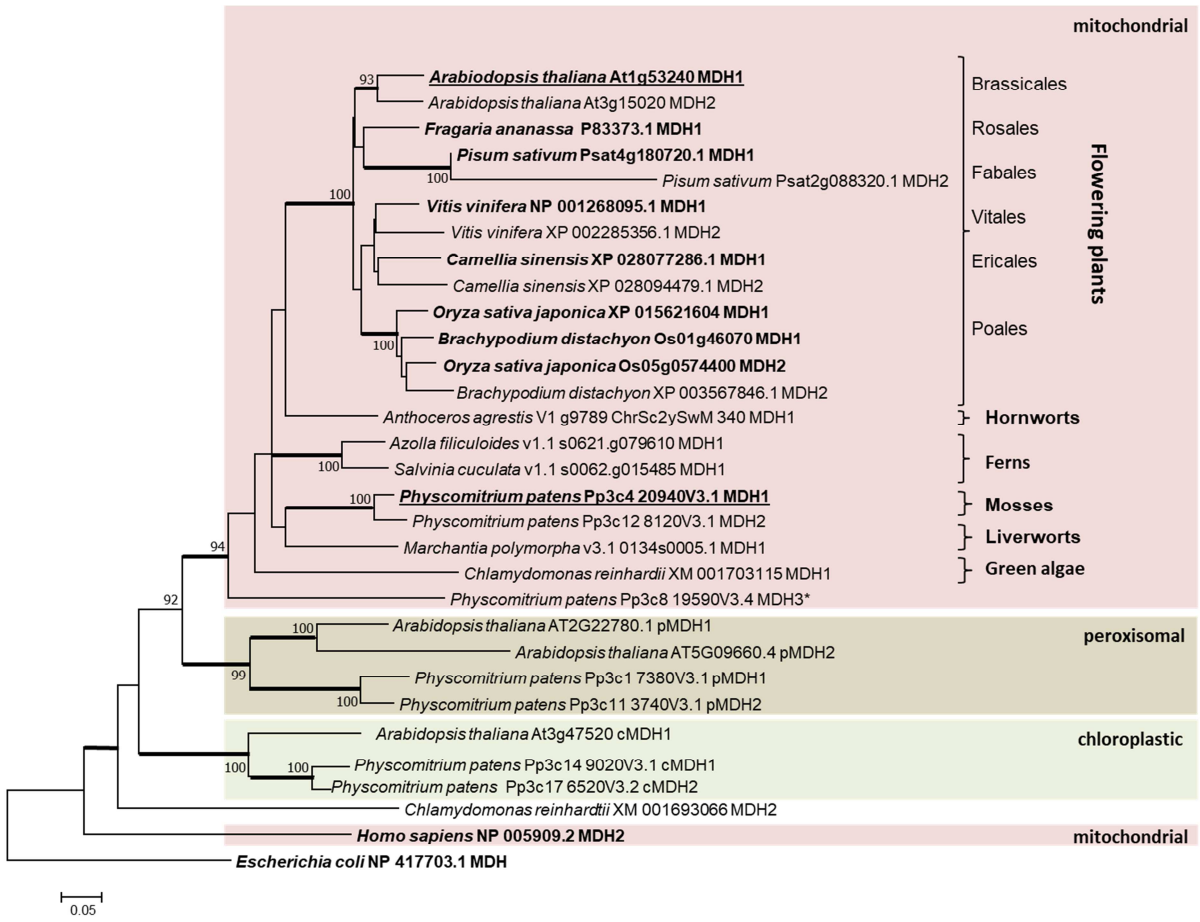

Supplementary Figure 1. Mitochondrial malate dehydrogenases along land plant phylogeny. Homologs of *A. thaliana* mMDH1 protein were extracted from available sequence data of model species of the main land plant clades. mMDHs of plant species with information on their lysine acetylation status as well as chloroplastic (cMDH) and peroxisomal (pMDH) MDHs of *A. thaliana* and *P. patens* are included. The human mMDH2 and *E. coli* MDH were used as outgroup to root the Neighbor joining tree with 1000 Bootstrap iterations. Bootstrap values are shown where exceeding 90.Thickened internode lines indicate bootstrap supports of 99-100 % in the Maximum likelyhood analysis calculated in parallel. For most species two paralogs of mMDHs were identified and labeled as MDH1 (dominant isoform) and MDH2. Isoforms for which acetylation sites were identified to date are labeled in bold, MDH proteins which are objects of this study are underlined. Red box: mitochondrial MDHs (mMDH), green box: chloroplastic MDHs (cMDH), brown box: peroxisomal MDHs (pMDH). For all proteins, species name is followed by accession number of the sequence or gene name (if accessible) and abbreviation. * marks a third MDH paralog (MDH3) encoded in the *P. patens* genome, which was not identified in the available proteomic datasets ((Müller et al., 2014) and this study). Analysis of sequence conservation and expression profiles suggest that MDH3 is likely an unfunctional protein (PEATmoos.org, (Fernandez-Pozo et al., 2020).

Supplementary Table 5. Lysine acetylome data of mMDH proteins in plants. Gene, protein and sequence information of the mMDH proteins of these species are listed as well as the name used for the protein in this study and the tissue, the proteins were isolated from in the cited publication. Acetylation sites are numbered based on their positions in the individual proteins (acK) and based on the corresponding position in the *A. thaliana* MDH1 protein (acK (AtMDH1)). Acetylation sites which are shared between two or more species are displayed in bold and underlined. *: Same peptide as in MDH1.

Species	Sequence information	name	Tissue/organ	acK	acK (AtMDH1)	Publication
Arabidopsis thaliana	At1g53240, Q9ZP06, AAG40021.1	MDH1	isolated mitochondria	170,325,329,334	**170**,325,**329,334**	König et al. 2014
			hda14/ WT leaves	identified, not acetylated		Hartl et al. 2017
				not identified		Uhrig et al. 2019
				170,325,329,334	**170**,325,**329,334**	all studies combined
	At3g15020, Q9LKA3	MDH2		170*	**170***	König et al. 2014
Camellia sinensis	XP_028077286.1_NCBI	MDH1	leaves	173, 187, 193	**169, 183**, 189	Jiang et al. 2018
	XP 028094479.1_NCBI	MDH2				
Vitis vinifera	F6HM78, RVW18853_NCBI	MDH1	fruit - mesocarp/exocarp - Lobesia botrana infection	39, 58, 135, 169, 178, 328	31, 50, 127, 161, **170**, 318	Melo-Braga et al. 2012
	XP_002285356.1 NCBI	MDH2				
Pisum sativum	Psat4g180720.1_URGI	MDH1	isolated mitochondria	138, 164	135, 161	Smith-Hammond et al. 2014
	Psat2g088320.1_URGI	MDH2				
Fragaria ananassa	P83373.1_NCBI	MDH1	leaves	180, 167	**170, 183**	Fang et al. 2015
Nicotiana tabacum			whole plant	not identified		Sun et al. 2017
Solanum tuberosum			seedlings	not identified		Salvatore et al. 2014
Glycine max			seedling leaves	not identified		Smith-Hammond et al. 2014
Triticum sativum			seeds	not identified		Zhang et al. 2016
Brachypodium distachyon (Bd21)	XP 003569456.1 NCBI	MDH1	seedling leaves	167	**169**	Zhen et al. 2016 Zhang et al. 2015
	XP 003567846.1 NCBI	MDH2		167*	**169***	
Oryza sativa ssp. japonicum	Os01g46070, Q94JA2, XP_015621604.1_NCBI	MDH1	seeds / embryos	333	**334**	He et al., 2016
	Os05g0574400, Q6F361, XP_015639465.1_NCBI	MDH2	leaves	166,180, 327	**169, 183, 329**	Zhou et al. 2018
			rice plant	not identified		Nallamilli et al. 2014
			seed embryos	167, 180, 327, 335	**170, 183, 329**, 337	He et al., 2016
			pistil/developing seeds	not identified		Wang et al., 2017
			complete rice plant	335	337	Xiong et al. 2016
				166, 167, 180, 327, 335	**169,170, 183, 329**, 337	all studies combined
Physcomitrium patens	Pp3c4 20940V3.1	MDH1	gametophore	172	**169**	this study
	Pp3c12 8120V3.1	MDH2	gametophore	170*	**169***	this study
	Pp3c8_19590V3.4	MDH3	gametophore	not identified		
Homo sapiens	P40926, NP_005909.2	MDH2		185, 301, 307, 314	190, 306, 312, 319	Wang et al.

						2010
Escherichia coli	P61889, NP_417703.2	MDH	*Escherichia coli*, different strains	54,56, 99, 107, 111, 133, 140, 162, 204, 272, 279, 300, 301	81, 83, 127, 135, 139, 161, 168, 190, 233, 301, 308, **329**, 330	Schilling et al. 2015
			Escherichia coli O139:H28 (strain E24377A / ETEC)	54,56,111,204,300	81, 83, 139, 233, **329**	Kuhn et al. 2014
			Escherichia coli O127:H6 (strain E2348/69 / EPEC)	99, 107,133, 140, 162, 272, 279, 301	127, 135, 161, 168, 190, 301, 308, 330	Kuhn et al. 2014
			Escherichia coli	99, 140, 162, 272, 300, 301	127, 161, 190, 301, **329**, 330	Bienvenut et al. 2020
				54,56, 99, 107, 111, 133, 140, 162, 204, 272, 279, 300, 301	81, 83, 127, 135, 139, 161, 168, 190, 233, 301, 308, **329**, 330	all studies combined

Supplementary Table 6. Primers used in this work.

Name	Sequence
mmdh1_GibFw	5´TACCATGGGCAGCAGCCATCACCATCATCACCAAC AGCCAGGATCCGGAAAGTCGCCATCCTTGG-3´
mmdh1_GibRv	5´GCAAGCTTGTCGACCTGCAGGCGCGCCGAGCTCGA ATTCGTCACTGGTTGGCAAACTTG-3´
mmdh1amb170_fw	5´- TAGTTGTTTGGTGTTACCACTCTTG-3´
pET16b_mmdh1_170_rv	5´- CTTTTCATCGTACATACCAGCCTTC-3´
mdh1amb325_fw	5´- TAGCCAGAACTCAAGTCCTCC-3´
pET16b_mmdh1_325_rv	5´- CAATGCTTCCAAGCCTTCCTTC-3´
mdh1amb329_fw	5´- TAGTCCTCCATAGAAAAGGGAGTC-3´
pET16b_mmdh1_329_rv	5´-GAGTTCTGGCTTCAATGCTTCC-3´
mmdh1amb325+newF	5´- TTGTAGCCAGAACTCTAGTCCTC-3´
mmdh1amb325+newR	5´- TGGCTACAATGCTTCCAAGCCT-3´
mmdh1amb329+newF	5´- CAGAACTCTAGTCCTCCATAGAATAGG-3´
mmdh1amb329+newR	5´- GACTAGAGTTCTGGCTTCAATGC-3´
mmdh1amb334newF	5´- TAGAATAGGGAGTCAAGTTTGCCAAC-3´
mmdh1amb334newR	5´- GACTCCCTATTCTATGGAGGACTTG-3´
MfeI_PpMDH1_f	5´- GGGCAATTGATGTCGTCGCAGACTCCCAAG-3´
KpnI_PpMDH1_r	5´- CTCGGTACCACTTCAAGCCTTCACATTCACG-3´
PpMDH1_KStop_f	5´- GGTACTTATGATCCCTAGAGGCTTTTTGGTGTC-3´
PpMDH1_KStop_r	5´- GACACCAAAAAGCCTCTAGGGATCATAAGTACC-3´
pCDFpylTfor	5´- TATTGTACACGGCCGCATAATCG-3´
pCDFpylTrev	5´- CAGCAGCCTAGGTTAATTAAGC-3´
BamHIXaMfeIfor	5´- GATCCGCATATCGAAGGTCGTC-3´
BamHIXaMfeIrev	5´- AATTGACGACCTTCGATATGCG-3´